Mutations in specific domains of MT5-MMP prevent the accumulation of toxic APP metabolites and serve as templates for peptide-based therapeutics in human in vitro models of Alzheimer's disease

Pedro Belio-Mairal, Athina Kamitsou, Delphine Stephan, Nicolas Jullien, Diarra Thiane, Melissa Ramos, Laurence Louis, Florian Benoist, Bastien Serrano, Marion David, et al.

Mutations in specific domains of MT5-MMP prevent the accumulation of toxic APP metabolites and serve as templates for peptide-based therapeutics in human *in vitro* models of Alzheimer's disease

Belio-Mairal P[1], Kamitsou A[1], Stephan D[1], Jullien N[1], Thiane D[1], Ramos M[1], Louis L[1], Benoist F[2], Serrano B[2], David M[2], Khrestchatisky M[1], Lécorché P[2], Nivet E[1], Rivera S[1]*.

1. Aix-Marseille Univ, CNRS, INP, Inst Neurophysiopathol, Marseille, France

2. Vect-Horus S.A.S., Faculté de Médecine, Marseille, France

* Corresponding author, santiago.rivera@univ-amu.fr

ABSTRACT

In previous work we identified key roles of membrane-type 5-matrix metalloproteinase (MT5-MMP) in Alzheimer's disease (AD) pathogenesis. More specifically, we uncovered the involvement of the C-terminal domains of the proteinase in the processing of amyloid precursor protein (APP) and the fate of some of its major toxic metabolites (*e.g.,* C99, Aβ). We further described these effects as being dependent on MT5-MMP transmembrane (TM) and intracellular (IC) domains, leading us to hypothesize that modifications in these domains could represent a therapeutic strategy to modulate toxic APP metabolites. To test this, here we generated MT5-MMP variants carrying amino acid deletions or substitutions in entire proteinase domains or in selected amino acid clusters in the IC domain. MT5-MMP variants were co-transfected in human cell lines overexpressing C99, reminiscent of an AD setting. We have identified mutations in the IC domain that induce C99 degradation and a decrease in Aβ levels, while other mutations have divergent effects on these APP metabolites. Furthermore, high content imaging revealed the importance of MT5-MMP IC modifications in C99 subcellular trafficking through the endomembrane system and how this impacts C99 processing. Proximity ligation assays also highlight the importance of the IC domain in MT5-MMP co-localization, and possible interaction, with C99. In a translational effort, we synthetized and functionalized a peptide mimicking the MT5-MMP IC domain carrying mutations in the N-terminus. We demonstrated that this synthetic peptide efficiently decreased C99 levels in our AD *in vitro* model. Overall, our study highlights the role of a selected group of amino acids in the C-terminal domains of MT5-MMP as the basis for a better understanding of the proteinase's contribution to APP metabolism. Moreover, this study provides a new approach for designing peptide-based therapeutic strategies against AD based on the properties of specific MT5-MMP domains to prevent C99 and Aβ accumulation.

INTRODUCTION

Matrix metalloproteinases (MMPs) form a multigenic family of endopeptidases with more than 20 members that display a wide spectrum of biological activities[1]. Membrane-type 5-matrix metalloproteinase (MT5-MMP, also known as MMP-24 or η-secretase), is the only MMP family member that is primarily expressed in neural cells[2,3] and contributes to a number of physiological and pathological processes in the nervous system[4,5]. Early studies demonstrated that MT5-MMP catalytic activity is required for the proper cleavage of extracellular and non-extracellular matrix proteins[5], playing a role in synaptic plasticity[6], neural stem cell differentiation[7], post-lesion synaptic reorganization[8], and axonal growth and regeneration[9].

The presence of MT5-MMP in amyloid plaques of Alzheimer's disease (AD) patients implied its possible implication in the disease pathogenesis[2]. Accordingly, MT5-MMP was found to cleave amyloid precursor protein (APP) in HEK cells[10] and murine primary neurons[11]. APP is central to the amyloid hypothesis of AD, as its processing by β-secretase generates the APP C-terminal fragment (CTF), C99, and its subsequent cleavage by γ-secretase releases the beta-amyloid peptide (Aβ)[12], which is the main constituent of amyloid plaques and a primary pharmacological target. APP cleavage was reduced in the brain of the 5xFAD mouse model of AD deficient in MT5-MMP, indicating the *in vivo* cleavage of APP by this MMP[13]. In addition, MT5-MMP deficiency in 5xFAD mice reduced the levels of Aβ and its immediate precursor C99, as well as the levels of neuroinflammatory mediators and glial reactivity, while long-term potentiation (LTP) and cognitive performance were preserved[13,14]. Furthermore, in favor of MT5-MMP involvement in AD pathogenesis, its overexpression in HEKswe cells caused the accumulation of C99 and Aβ[13]. Moreover, MT5-MMP cleavage of APP at the η-site releases η-CTFs, which carry synaptotoxic activities[15] and contribute to Aβ production[16].

Considering their increasing pathological relevance in AD, the functional interaction of MT5-MMP and C99 is of great interest. C99 buildup precedes that of Aβ in the 3xTg and 5xFAD mouse models of AD[17,18]. In humans, C99 accumulates in brains of patients with AD[19], as well as in neurons carrying familial AD mutations, leading to endosomal dysfunction[20]. We recently reported that MT5-MMP controls the metabolism of APP and its CTFs *via* both

dependent and independent proteolytic mechanisms, indicating that certain non-catalytic domains are important for regulating its functions, particularly its interactions with APP[4].

In this study, we aimed to gain a better understanding of the mechanisms underlying the control of C99 by the non-catalytic domains of MT5-MMP. We used molecular and cell biology, and structure-function approaches, to assess the relevance of specific amino acid residues in the fate of C99 and Aβ. We provide new insights into the functional interactions between MT5-MMP and C99 and provide new perspectives for adopting MT5-MMP-based therapeutic strategies to modulate C99 in mammalian cells.

MATERIALS AND METHODS

Plasmid constructs

All plasmids were constructed using a pcDNA3.1 backbone. The new plasmids used in this study (ΔEXT, TM1/IC5, TM5/IC1, all the mutated variants of TM/IC) (Fig 1A, 2A) were generated by GeneArt (ThermoFisher Scientific). Constructs encoding other MT5-MMP variants (pcDNA, TM/IC, EXT/TM, EXT) and C99 or HA-C99 were produced as previously described[4]. Plasmids were purified and amplified as previously described[4].

Cell lines

HEK cells were maintained with DMEM Glutamax (61965026, ThermoFisher Scientific) supplemented with 10% fetal bovine serum (FBS) (A3160801, ThermoFisher Scientific) and 1% penicillin/streptomycin (15140122, ThermoFisher Scientific) (hereafter referred as HEK media). For the passaging procedure, cells were washed with 5mL of DPBS (14190094, ThermoFisher Scientific) and 2 mL of 0.05% Trypsin-EDTA (25300054, ThermoFisher Scientific) were added for 2 min. Next, 8 mL of HEK medium were added to a T75 flask (353136, Corning), and cells were dissociated into single cells by gentle mechanic pipetting. Then, 3 mL of the cell suspension was replated in a new T75 flask containing 10 mL of fresh HEK medium. Geneticin (10131027, ThermoFisher Scientific) was added at a 1:100 dilution.

hTERT-RPE1 cells were cultured using the same protocol used for HEK cells but with different reagents. The medium consisted of DMEM/F12 (31331028, ThermoFisher Scientific)

supplemented with 10% FBS and 1% penicillin/streptomycin. HBSS (14025050, ThermoFisher Scientific) was used for washing. Moreover, 0.25% Trypsin-EDTA (25200056, ThermoFisher Scientific) was used for 5 min to dissociate the cells.

Transfections

The cell lines were transfected using JetPei® Polyplus (101000053, Sartorius). For 24-well plate (353047, Corning) and 96-well plate (6055300, Revvity; 353072, Corning) formats, reverse transfection (the plasmids are added to the plate and the cells are then seeded onto it) was used to limit toxicity and increase transfection efficiency in low cell density context (< 15,000 cells/well). For larger volumes or densities, classical forward transfection was used. In both cases, the manufacturer's instructions were followed with the recommended volumes of transfection reagents and DNA quantities. The cell densities were adjusted according to the cell line. HEK cells were seeded in 6-well plates (353046, Corning) at a density of 1.5 M per well. hTERT-RPE1 cells were seeded at 10 K per well in 96-well plates and 25K in 24-well plates.

All the inhibitors were diluted in DMSO (D2650, Sigma-Aldrich). Inhibitors (Table 1) were added 15–17 h after transfection. After 20 h, cells were lysed and collected for experiments.

MTT test

HEK cells were seeded at 50,000 cells/well in 96-well plates according to the recommended volumes per the JetPei Polyplus protocol. The next day, cells were transfected or treated with the corresponding peptides. At 48 h after transfection or peptide treatment, 25 µL/well of a 5 mg/mL solution of Thiazolyl Blue Tetrazolium Bromide (M5655, Sigma-Aldrich) in HEK medium were added to each well to obtain a final solution of 0.5 mg/mL. After 3 h of incubation, the culture medium was aspired, and the formazan crystals were dissolved in 100 µL/well dimethyl sulfoxide (DMSO) (D2650, Sigma-Aldrich). The plates were shaken in the dark until the crystals were fully dissolved. Finally, the plates were read in

a multiwell plate reader with an emission filter of 544-10 nm with 3 mm diameter of orbital averaging, and 10 flashes per well.

To analyze the absorbances, the average of each row and column was used to normalize technical differences and differences in plate reading. Then, the condition with the transfection reagent but without the plasmid or peptide was used as a normalizing control for all readings to compare the different biological conditions.

Protein quantification

A bicinchoninic acid assay was used to quantify the protein concentration in the cell lysates. A BCA assay kit was used (23225, ThermoFisher Scientific) following manufacturer's instructions for the multiwell plate format. Lysates from HEK cells were diluted 1:5 with lysis buffer to enter the detection range of the kit. The samples for the standard curves were obtained from a ready-to-use BSA standard kit (23208, ThermoFisher Scientific). Each multiwell plate contained the standard curve dilutions with a blank for each lysis buffer used and the different samples. All measurements were performed in two technical replicates and, when possible, standard curve dilutions and blanks were performed in triplicate. Absorbance was measured using a multiwell plate reader with a 544-10 nm emission filter.

The standard curve was calculated using the 4-parameter fit of MARS data analysis software version 2.10R3 (BMG Labtech). Concentrations were extrapolated using the same software to calculate the volumes necessary for downstream applications.

Western Blot

After protein quantification, 20 µg of protein in 15 µL for 10-well gels or 7.5 µL for 15-well gels were prepared with ultrapure H_2O (0066571E, B.Braun). Samples were mixed with the same volume of 2x Tris-Glycine (LC2676, ThermoFisher Scientific) or Tricine (LC1676, ThermoFisher Scientific) sample buffer and heated at 95°C for 5 min or 85°C for 20 min for small-sized (<20 kDa) target proteins.

The overall protocol of western blot is based on ThermoFisher's instructions using a Mini gel tank system (A25977, ThermoFisher Scientific) and a Power Blotter Semi-dry Transfer

system (PB0013, ThermoFisher Scientific). All products cited in this section were obtained from ThermoFisher Scientific unless otherwise stated. Specifically, Novex 4-20% Tris-Glycine gels with 10 wells (XP04200BOX) or 15 wells (XP04205BOX) were run at 40 mA per gel with a maximum voltage of 130 V for 1h30 or until the 10 kDa marker of the prestained protein ladder (26616) was at the lowest end of the gel. Novex 16% Tricine gels with 10-well (EC6695BOX) or 15-well (EC66955BOX) formats were used with a Multicolor Low Range protein ladder (26628), and they were run at 80 mA per gel with a maximum voltage of 130 V for 1 h 30 min or until the 10 kDa marker reached the lowest end of the gel.

The gels were transferred into 0.45µM nitrocellulose blotting membranes (10600002, Amersham) assembled with two stacks of five units of 0.34-mm Whatman papers (3030-917, Cytiva) on top of the gels and another stack below the membranes. Prior to building the stack, all components were wetted with Towbin buffer composed of double-distilled H_2O (ddH_2O) with 25 mM Tris-Base (T1503, Sigma-Aldrich), 192 mM Glycine (G8898, Sigma-Aldrich), and 20%$_{v/v}$ methanol (34860, Sigma-Aldrich) at a final pH of 8.3 ± 0.1. The stacks were then arranged in the PowerBlotter and ran in standard semi-dry mode (25 V with 1 A maximum) for 1 h.

Blotting membranes were recovered and incubated in Ponceau solution (P7170, Sigma-Aldrich) for 30 s. Ponceau staining was captured using the Preview mode on a NineAllience 9.7 17.02 (UVITec). The membranes were then blocked for 1 h in agitation at room temperature with a blocking buffer consisting of 1x PBS (ET330-A, Euromedex) with 5%$_{m/v}$ powder milk and 0.2%$_{v/v}$ Tween20 (P1379, Sigma-Aldrich). Afterwards, antibodies were diluted to 1:1000 (anti-actin antibodies were diluted 1:5000) in blocking buffer and transferred with membranes to a clean recipient for incubation overnight at 4°C with agitation. The next day, the membranes were washed 3 times for 10 min under agitation at room temperature with 1x PBS and 0.2%$_{v/v}$ Tween20 (washing buffer). The membranes were incubated with HRP-conjugated secondary antibodies (1:1,000) in blocking buffer for 1 h under agitation at room temperature. After 3 washes of 10 minutes each with wash buffer, ECL solution (RPN2106, Amersham) or ECL Prime solution (RPN2236, Amersham) was used as per the manufacturer's instructions, depending on the signal intensity, and the membranes were visualized using the chemiluminescence mode of the UVITec station.

The western blot bands were semi-quantified using Fiji's tool "Plot lanes" from the "Gels" module[21]. The actin band values were used to normalize the remaining values.

Immunocytochemistry

Cells were cultured in 12-mm glass coverslips for confocal microscopy (65.300.21, Dutscher), 1.5H coverslips for super-resolution microscopy (0117520, Marienfeld Superior), or 96-well plates (6055300, Revvity) for high-content screening microscopy.

For sample fixation, PEM buffer was prepared to obtain a final solution of PIPES 80 mM (P1851, Sigma-Aldrich), $MgCl_2$ 2mM (M9272, Honeywell), and EGTA 5mM (E4378, Sigma-Aldrich) at pH 6.8 in ddH_2O. Then, paraformaldehyde (15714, Electron Microscopy Services) was diluted at 4%$_{v/v}$ in PEM with 4%$_{m/v}$ sucrose (S0389, Sigma-Aldrich) (fixation solution).

Glass coverslips 12 mm in diameter were washed with 0.5 mL of 1x DPBS previously to adding 300µL/well of fixation solution at room temperature. After incubating the cells for 10 min at room temperature, they were washed 4 times with 0.5 mL of DPBS. Cells were later blocked and permeabilized for 1 h under gentle agitation at room temperature with 3%$_{m/v}$ bovine serum albumin (BSA) (A7906, Sigma-Aldrich), 0.1% Triton X-100 (X-100, Sigma-Aldrich), and 10% normal goat (005-000-121, Jackson ImmunoResearch) or donkey (017-000-121, Jackson ImmunoResearch) serum in 1x DPBS (block/per buffer). For organelle staining, Triton X-100 was replaced with saponine (84510, Sigma-Aldrich) at the same concentration. After blocking and permeabilization, primary antibodies were diluted to the corresponding concentrations (Table 2) in block/per buffer. Cells were incubated with diluted antibodies overnight at 4°C.

The next day, cells were washed 3 times with 1x DPBS for 5 min under gentle agitation at room temperature. The secondary antibodies (Table 2) were diluted to 1:800 in block/per buffer, and cells were incubated with the diluted secondary antibodies for 1 h under gentle agitation at room temperature and protected from light. Then, cells were washed twice with 1x DPBS for 5 min under gentle agitation at room temperature and incubated for 10 min under the same conditions with 10 µg/mL Hoechst33342 (H3570, ThermoFisher Scientific) diluted in 1x DPBS. Finally, cells were washed twice more with 1x DPBS for 5 min under gentle agitation at room temperature, and coverslips were mounted on slides using 6µL of mounting media

(P36934, ThermoFisher Scientific). Slides were allowed to dry at room temperature overnight and curated at 4°C for 48 h before imaging.

For high-content imaging, the procedures were the same with adjusted volumes, except that the plates were parafilm-sealed and kept in DPBS after the two last DPBS washes following Hoechst 33342 incubation.

Microscopy analyses

Python procedures to clean, downsize, normalize, and visualize quantitative data from the automated microscope were run in Jupyter Notebooks (available at: github.com/RiveraLabINP/BelioMairal_2024). In brief, the overlap values of individual cells were retrieved from the Operetta© software (quantification workflow available at: github.com/RiveraLabINP/BelioMairal_2024). These values were multiplied by the area of HA fluorescence to generate a new variable representing the total area of overlap of HA with each organelle. The overlap areas were normalized using the standard values of the Power Transformer function from the sklearn package. The individual cells were then clustered using KMeans from sklearn package in 9 different clusters based on the overlap area and the number of HA spots in the cell. The dataset was downsized excluding the clusters of cells with the smallest and biggest values. The mean area of overlap was calculated for each MT5-MMP variant and normalized to the pcDNA value of each independent experiment. Finally, outliers were detected with the Tukey method by discarding values outside the fences using 1.5 as the outlier multiplier. The resulting values were used to visualize the results and Bayesian statistics.

Prior to principal component analysis, the values were standardized using the StandardScaler from the sklearn package. Once normalized and standardized, the PCA function from skleanr was used with two principal components (n components=2). For cluster analysis, the function clustermap from the seaborn package was used with the metric “canberra” (metric=‘canberra’).

A complete list of Python and package versions is provided at: github.com/RiveraLabINP/BelioMairal_2024.

ELISA

To measure secreted Aβ40 in our samples, an ELISA kit was used (KHB3481, ThermoFisher Scientific) following manufacturer's instructions. Briefly, culture supernatants were recovered in low-binding tubes (022431081, Eppendorf) and stored at -80°C or immediately used. Samples were centrifuged at 1400 rpm for 1 min at room temperature. The supernatants were transferred to new low-binding tubes, and the samples were diluted to match the detection range. The manufacturer's protocol was followed for the remaining procedures.

Absorbance was measured using a multiwell plate reader with an emission filter 450-10 nm and 10 flashes per well. The standard curve was calculated using the 4-parameter fit of the MARS data analysis software. Concentrations were extrapolated using the same software, and values from the pcDNA condition were used to normalize all other values to account for technical variability. Thus, the results are presented as fold-changes compared with cells co-transfected with empty pcDNA and C99 overexpression constructs.

Proximity ligation assay

Colocalization between C99 and MT5-MMP constructs was performed using DuoLink© In Situ system. All volumes were adjusted to perform the procedures in 96-well plates. The goat anti-rat (112-005-003, Jackson ImmunoResearch) and goat anti-rabbit (111-005-003, Jackson ImmunoResearch) unconjugated antibodies were conjugated with DuoLink© PLA orange probes (DUO96030-1KT, Sigma-Aldrich) following the manufacturer's instructions and stored at 4°C. Cells were stained using the normal immunofluorescence protocol until secondary antibody binding. Secondary antibody binding and further procedures were performed according to DuoLink© In situ orange detection kit (DUO92007-100RXN, Sigma-Aldrich). Finally, cells were stained with Hoechst 33342, as previously explained, and plates were sealed with parafilm.

Peptide synthesis and conjugations

Fmoc–amino acids were obtained from Iris Biotech (Marktredwitz, Germany). All other amino acids and reagents were purchased from Sigma-Aldrich (Saint-Quentin-Fallavier,

France) or Analytical Lab (Castelnau-le-Lez, France). Peptide assembly was performed using a Liberty (CEM®) microwave synthesizer by solid phase peptide synthesis (SPPS) based on the Fmoc strategy. Fmoc–Gly-Wang resin (loading 0.66 mmol/g) were purchased from Iris Biotech and were used as solid support.

Purification and analysis of peptide-based products

Monitoring of reactions and quality controls of the peptide-based intermediates were carried out by liquid chromatography/mass spectrometry (LC/MS) using a Thermo Fisher Scientific UltiMate®3000 system (Waltham, MA, USA) equipped with an ion trap (LCQ Fleet) and an electrospray ionization source (positive ion mode). The LC flow rate was set to 2 mL/min using H2O 0.1%TFA (buffer A) and MeCN 0.1%TFA (buffer B) as eluents. The gradient elution was 10%–90% B in 10 min (quality control) equipped with a C18 Kinetex™ (2.6 µm, 50 mm × 4.6 mm). The heated electrospray ionization source had a capillary temperature of 350 °C. Crude peptides were purified using reverse-phase (RP)-High Pressure Liquid Chromatography (HPLC) on a Thermo Fisher Scientific UltiMate®3000 system equipped with a C18 Luna™ (5 µm, 100 mm × 21.2 mm). The detection was performed at 214 nm. The elution system comprised H2O 0.1%TFA (buffer A) and MeCN 0.1%TFA (buffer B). Flow rate was 20 mL/min.

Preparation of p17 and p20

Peptide p17: H-QFAAAAAPQPVTYYKRPVQEWV-COOH and peptide p20: H-QFKNKTGPQPVTYYKRAAAEWV-COOH were synthesized using 0.1 mmol SPPS Fmoc–Gly-Wang resin under microwave activation. Resin was swollen in DMF for 10 min. Deprotection of the fmoc-protecting group was performed using a solution of 20% piperidine in DMF for 200 s under microwave activation at 75 °C. Stepwise assembly of the Fmoc–protected-amino-acids were performed under microwave activation using standard Fmoc peptide chemistry. Double coupling times of 240 s were used with a solution of Fmoc–amino acid (1 eq), Oxyma (10 eq excess; 1 M) in DMF, and DIC (5 eq excess; 1 M) in DMF under microwave activation at 90 °C. Double coupling was used for R amino acids to improve yield. Finally, the peptidyl-resin was washed 3 times with DCM and then treated with TFA/TIS/H2O

(95:2.5:2.5) containing DTT (10 mg/1mL) at room temperature for 4 h. The cleavage solution was recovered, concentrated under N2 flow, precipitated with cold diethyl ether and washed 2 times with cold diethyl ether. The crude products were dissolved in an H2O + 0.1%TFA /MeCN + 0.1% TFA (1:1) mixture and lyophilized. The crude peptide was purified using preparative RP-HPLC as described previously to obtain p17 and p20 as white powders (p17: 60 mg, 24%; p20: 52 mg, 20%).

Production of VHH C5

Phagemid encoding VHH C5 was transformed in the E. coli BL21DE3 strain. Transformed bacteria were grown in 200 ml of 2YTA until 0.5 < OD600 < 0.8 and induced with 100 µM IPTG overnight at 30 °C with shaking (250 rpm). Bacteria were pelleted and lysed by freeze-thawing and BugBuster® Protein Extraction Reagent (Novagen, Pretoria, South Africa). After a centrifugation step (3000 g, 20 min), VHH C5 was purified from the supernatant using metal affinity chromatography, TALON® Superflow™ (GE Healthcare), according to the manufacturer's instructions. Bound molecules were eluted with 250 mM imidazole, which was eliminated using PD-10 Desalting column (GE Healthcare). An additional gel filtration step using a Superdex 75 column (Cytiva, Marlborough, USA) was performed to remove endotoxins. The purified VHH was validated for its quality and purity by LC-MS on a Orbitrap Exploris apparatus (Thermo Fisher Scientific).

Chemical conjugation of VHH C5 and p17

First, C5-PEG2-BCN was prepared. An Eppendorf vial was filled with VHH C5 (8.0 mg, 539 nmol, 2.0 mL in PBS 1X), BCN-PEG2-NH2 (5.2 mg, 16170 nmol, 0.5 mL in PBS 1X) and BTG (10.8 U, 0.08 mL). The reaction mixture was left overnight at room temperature and purified by size exclusion chromatography hiload 16/600 Superdex 75 pg using PBS 1X as an eluent to give C5-PEG2-BCN as a colorless solution (6.8mg, 79%, 2.1mL in PBS 1X). Finally, in an Eppendorf vial were introduced respectively C5-PEG2-BCN (1.8 mg, 119 nmol, 557 µL in PBS 1X) and p17 (1.0 mg, 356 nmol, 234 µL in PBS 1X). The reaction mixture was left overnight at room temperature and purified by size exclusion chromatography Superdex 10/300

increase 75 GL using PBS 1X as eluent to give C5-p17 as a colorless solution (1.5mg, 72%, 290 µL in PBS 1X).

Statistics

Frequentist statistics were performed using GraphPad Prism 10.2.3 for MacOSX (GraphPad Software). Unless otherwise stated, all tests were ANOVA with Dunnett's post hoc multiple comparison test for comparison with the control condition of each experimental set. The same software was used to generate the graphs, where the p-values are represented with * p value < 0.05, ** p value < 0.01, *** p value < 0.001, and **** p value < 0.0001.

For Bayesian statistics, JASP 0.18.3 (JASP team) was used to perform Bayesian ANOVA with post hoc tests. Prior odds were unchanged from the software default values, and the Bayes factor was LogBF10 when compared with the null model.

All statistical analyses were performed using at least three independent experiments.

RESULTS

Modulation of C99 and Aβ levels by non-catalytic MT5-MMP variants

We previously showed that the removal of the MT5-MMP intracytoplasmic (IC) domain alone or together with the transmembrane (TM) domain, referred to as EXT/TM or EXT, drastically reduced C99 levels when either of these two constructs was expressed with a plasmid encoding C99 in HEK cells. In contrast, deletion of the extracellular domains (EXT) of MT5-MMP, here named TM/IC, was sufficient to reproduce pro-amyloidogenic effects of MT5-MMP in cells overexpressing C99[4]. Thus, we aimed to identify the specific residues in TM/IC that are responsible for C99 and Aβ accumulation. However, it was unclear whether proteolytic activity in the catalytic site of EXT could account for its anti-amyloidogenic effects. Accordingly, we rendered the truncated variant inactive by substituting the Glu283 residue of the catalytic site with alanine (hereafter referred as ΔEXT) (see Fig 1A for scheme of constructs). Following coexpression of MT5-MMP variants and C99, there was no decrease in cell survival (Fig 1B). However, western blot analysis using an anti-CTF antibody revealed a significant decrease of C99 levels by 83%, 71%, and 74% in cells expressing EXT, EXT/TM, and ΔEXT, respectively, compared with our pro-amyloidogenic control MT5-MMP TM/IC (Fig 1C). This indicates that the catalytic activities of EXT and EXT/TM are not responsible for the significant drop in C99 levels in the absence of the TM and IC domains. Under these conditions, we also observed a significant decrease in the supernatant Aβ levels of cells expressing EXT, as assessed by ELISA, whereas ΔEXT cells exhibited Aβ levels close to control values (Fig 1D). This suggests that the inactivation of the catalytic domain may drive part of C99 toward Aβ production, contrary to EXT.

Next, we sought to elucidate whether the effects on C99 modulation were primarily due to the exclusion of the TM or IC domain, or both. To this end, we generated whole-domain substitutions to explore whether selective modifications of the MT5-MMP TM or IC amino acid sequences were sufficient to cause a significant reduction in C99 levels. Substitutions were based on previously reported functional divergencies between MT5-MMP and MT1-MMP, where suppression of the IC domain of MT1-MMP caused a strong increase in C99 levels, in contrast to the decrease caused by suppression of the MT5-MMP IC domain herein confirmed [4]. Accordingly, we generated two chimeras combining the TM and IC domains of both

proteinases: one construct encoding the TM of MT5-MMP and the IC of MT1-MMP (namely TM5/IC1) and another with the reverse composition (TM1/IC5) (see Fig 1A). The coexpression of TM5/IC1 or TM1/IC5 constructs with C99 had contrasting effects on both C99 and Aβ levels, but no effect on cell survival (Fig 1B, E, F). On the one hand, TM5/IC1 maintained C99 levels while drastically reducing Aβ secretion by 67% (Fig 1E, F). On the other hand, TM1/IC5 significantly decreased C99 levels by 69% but maintained Aβ levels similar to those of control TM/IC (Fig 1E, F). Overall, the contrasting outcomes for C99 and Aβ with both chimeras indicate a distinct influence on C99 processing, depending on the presence of MT5-MMP TM or IC.

MT5-MMP non-catalytic variants control C99 processing

We next investigated the fate of C99 by modulating two of the main C99 degradation systems, lactacystin (LACT) to inhibit proteasome activity and ELND006 (D6) to inhibit γ-secretase. In EXT-expressing cells, we found that only LACT treatment caused a significant recovery of C99 levels, whereas D6 had no effect (Fig 1G), indicating a prominent role of proteasome over γ-secretase in C99 degradation upon co-expression with EXT. Similarly, in the ΔEXT group, treatment with LACT also induced a significant recovery of C99, whereas D6 failed to rescue C99 levels (Fig. 1H). Considering that coexpression of ΔEXT with C99 maintains Aβ levels, the lack of recovery of C99 with D6 suggests the possibility of EXT catalytic activity in impeding Aβ generation.

Our previous studies demonstrated that treatment of HEK cells with Bafilomycin A1 (BAFA1)—an inhibitor of the V-ATPase pump[22]—increased C99 in the presence of MT5-MMP TM/IC but decreased C99 in the presence of EXT, indicating that C99 is processed in the autophagolysosome pathway in a context of high Aβ production in HEK cells expressing TM/IC [4]. BAFA1 treatment induced a significant 331% recovery of C99 levels in ΔEXT-cotransfected cells, an effect that remained well below the recovery of LACT. In contrast, BAFA1 had no significant effect in EXT-expressing cells (Fig 1G, H). Therefore, the inactivation of the MT5-MMP catalytic domain along with the deletion of the TM and IC domains partially drives C99 into lysosomal compartments, although proteasomal degradation is predominant. This confirms that the proteasome is the primary processing machinery of C99

in the presence of EXT or ΔEXT, with an alternative degradation pathway involving EXT catalytic activity in lysosomal compartments. However, other enzymes present in lysosomes could also be responsible for Aβ increase in ΔEXT-expressing HEK cells.

The lysosomal enzyme cathepsin B can cleave and degrade Aβ[23]. In addition, cathepsin B colocalized with C99 in enlarged lysosomal structures and cleaves APP-CTFs at C-terminal sites, thereby removing the C99 CTF epitope[17,24]. Thus, we postulated that cathepsin B could be a potential generator of Aβ peptides detected by ELISA. However, this hypothesis was not supported after using CA-074-Me (CA074), a well-known cathepsin B inhibitor, which had no effect on canonical APP secretases[24]. This failed to recover C99 levels in EXT- or ΔEXT-expressing cells (Fig 1G, H), suggesting that inhibition of a single lysosomal enzyme is insufficient to restore C99 levels and block Aβ production.

We next used LACT and D6 to identify the main C99 processing pathways for each chimera to better understand the mechanisms underlying their differences. The outcome of C99 expression in both chimeras was completely different. Neither LACT nor D6 changed C99 levels in the presence of TM5/IC1, which was maintained close to the control DMSO-treated condition (Fig 1I). In contrast, LACT and D6 drastically increased C99 levels by 212% and 323%, respectively, when expressing the TM1/IC5 variant (Fig 1J), suggesting that both the proteasome and the γ-secretase mediate the reduction in C99 levels observed in this chimera.

Specific amino acid deletions in the IC domain reduce C99 and Aβ levels

We next investigated whether the deletion of specific IC residues could mimic the decrease in C99 levels caused by the deletion of the entire IC domain. We deleted a series of amino acids in the MT5-MMP IC domain that differed from those in MT1-MMP IC, owing to the potential role of these amino acids in the opposite effects of suppressing the IC domain of MT5-MMP and MT1-MMP as previously reported[4]. From N-terminal to C-terminal, the deletions were: KNKTG, QPVT, YK, PVQ, and EWV (Fig 2A). None of the mutations induced cytotoxicity in HEK cells expressing these constructs with C99 (Fig 2B). On average, specific deletions in the MT5-MMP IC domain tended to reduce C99 levels by 40% ± 10%, but this

decrease was insufficient to achieve statistical significance (p-values between 0.1 and 0.5) with the exception of KNKTG deletion, which significantly reduced C99 levels by 53% (Fig 2C).

Sequence substitutions in the IC domain modulate C99 and Aβ levels

The minimal differences observed in C99 levels following targeted deletions could imply changes in IC conformation that ultimately interfere with the physiological effects of MT5-MMP. We hypothesized that alanine (ala) substitutions in different groups of amino acids could better preserve the IC conformation while revealing possible functional effects of the mutations for a given group. In addition, we generated a construct in which all selected amino acids were simultaneously substituted with ala. Similar to the deletions, the substitution of specific residues with ala exhibited no effects on cell survival (Fig 2B). Upon coexpression with C99 in HEK cells, only the constructs with the substitution of KNKTG or PVQ groups exhibited significant reductions (69% and 51% respectively) in C99 levels compared with the TM/IC control, as revealed by WB using the anti-CTF antibody (Fig 2D). Seemingly, ala substitutions of all selected residues significantly decreased C99 levels by 69% (Fig 2D). In contrast, ala substitutions in the PDZ-binding EWV motif maintained high C99 levels equivalent to those of TM/IC (Fig 2D).

Only KNKTG substitution translated the C99 reduction into a significant decrease (72%) in Aβ levels (Fig 2E). Substitutions in PVQ or all targeted groups were insufficient to modulate Aβ levels, which remained close to control levels. Thus, KNKTG remained as the key amino acids for halting C99 and Aβ accumulation in HEK cells overexpressing C99, whereas EWV ala substitution preserved the same pathologic profile in both C99 and Aβ as TM/IC control.

Decreased C99 levels after KNKTG substitution in MT5-MMP IC could result from changes in the proteolytic degradation of C99. Thus, we treated HEK cells with LACT and D6 after co-transfection with C99 and one of the following: TM/IC or TM/IC(ala)KNKTG or TM/IC(ala)EWV. On the one hand, both LACT and D6 significantly restored the expression of C99 when co-transfected with TM/IC (Fig 2F). On the other hand, C99 levels in the TM/IC(ala)KNKTG group remained unchanged upon treatment with LACT or D6 (Fig 2G), suggesting an alternative degradation pathway to proteasome or γ-secretase. In HEK cells co-transfected with TM/IC(ala)EWV, D6 but not LACT increased C99 levels, highlighting the

importance of γ-secretase processing of C99 in the presence of TM/IC(ala)EWV and no proteasomal degradation (Fig 2I). These significant changes in the fate of C99 could reflect the translocation of MT5-MMP variants into subcellular compartments that facilitate C99 processing by specific proteases.

MT5-MMP variants alter the patterns of subcellular localization of C99

To determine the possible influence of MT5-MMP variants on C99 distribution and therefore on its metabolism, we co-transfected human retinal pigment epithelial cells (RPE1) with HA N-terminally tagged C99 (HA-C99) and MT5-MMP variants known to differentially modulate C99 processing (Fig. 3A). RPE1 are highly adherent and of an optimal size to facilitate microscopic observations at the subcellular level. In addition, these cells do not express detectable levels of MT5-MMP (Fig. 3B) and, similarly as neural cells, have an embryonic neuroectodermal origin[25]. We used anti-HA antibodies to detect HA-C99 and specific antibodies targeting different cell organelles from the endomembrane system (early endosomes, Golgi apparatus, endoplasmic reticulum, and lysosomes) to investigate HA-C99 subcellular localization using immunofluorescence. We acquired and analyzed the images using quantitative unbiased high content screening microscopy (HCS). We used pcDNA as a reference construct with respect to HA distribution for data normalization and calculated the increase or decrease in the percentage of MT5-MMP variants relative to pcDNA.

The distribution of the HA signal substantially changed under the influence of different MT5-MMP variants (Fig. 3C), indicating distinct distribution patterns. Notably, all MT5-MMP variants caused an overall reduction in HA signal within the Golgi apparatus (27%±12) and the endoplasmic reticulum (14%±6) relative to pcDNA control. In contrast, we observed inconsistent changes in HA signal among MT5-MMP variants in early endosomes (10%±10), accompanied by a slight increase (11%±9) in the lysosomal HA signal (Fig 3C). However, absolute quantification is insufficient to understand the complexity of HA signal distribution in different organelles and under the influence of different MT5-MMP variants.

To visualize our data structure that summarizes the effects of the MT5-MMP variants on C99 distribution, we conducted principal component analysis (PCA) using two principal components, which collectively account for 75% of the total variability of the HA signal (Fig

3D). We observed that pcDNA and TM/IC(ala)EWV were isolated from the other MT5-MMP variants, indicating that coexpression of these two constructs leads to different HA-C99 distribution patterns in heterologous cells. In addition, three differentiated groups emerged within the main cluster: those with MT5-MMP TM (EXT/TM, TM/IC, TM/IC(ala)KNKTG), those lacking MT5-MMP TM (EXT, TM1/IC5), and the TM5/IC1 chimera positioned between these groups. These findings suggest: i) that HA-C99 distribution among different organelles varies depending on the coexpression of MT5-MMP variants, and ii) that the presence of MT5-MMP TM strongly determines HA-C99 subcellular localization.

To identify which MT5-MMP constructs significantly influenced the HA-C99 distribution in each organelle we performed a cluster analysis, using Bayesian ANOVA followed by multiple comparison tests. The natural logarithm of Bayes Factor 10 (LogBF10) quantifies the likelihood of differences in means between various groups, providing a measure of the posterior odds that the alternative hypothesis holds. In other words, it makes it easier to estimate the probability that means actually differ[26]. For instance, a LogBF10 value of -1.1 infers that the null hypothesis is three times more likely than the alternative hypothesis, 0 indicates the same probability for both, and a LogBF10 value of 1 indicates a probability approximately three times greater than the alternative hypothesis. This approach provides a quantitative criterion to evaluate differences between groups without the restrictions of conventional frequentist methods, which use p-values to interpret the data. However, this approach may overlook meaningful patterns in the data and is less informative[26]. In the context of our results, LogBF10 provides us with a quantitative framework to interpret whether the differences observed in the absolute quantification of HA signals are sufficient to reject or accept the null hypothesis. It indicates whether the means are equal or different, or if there is a lack of evidence (*i.e.* high variability, small number of repetitions, etc.) to draw a solid conclusion.

We calculated the sum of LogBF10 values for each comparison of the effect of individual MT5-MMP variants on HA-C99 expression in each organelle to create a cluster map that visually represents the strength of evidence for variability in different constructs across multiple organelles (Fig 3E, F). TM/IC(ala)EWV differed from other constructs in HA signal distribution within the Golgi (16.83), endoplasmic reticulum (2.15), and lysosomes (3.63). However, other MT5-MMP variants changed HA-C99 distribution in one or other specific

cellular compartments: TM1/IC5 in the endoplasmic reticulum (ER) (4.57), EXT/TM in the endosomes (4.30), and EXT in the Golgi (1.60) (Fig 3E, F).

MT5-MMP variants heterogeneously determine HA-C99 subcellular localization

Bayesian analysis indicated that all MT5-MMP constructs altered HA-C99 subcellular distribution compared with the pcDNA control, but certain MT5-MMP variants distinctly altered HA-C99 subcellular distribution in organelles. Thus, we delved deeper into the individual differences in HA signal in each organelle for each MT5-MMP construct by analyzing the LogBF10 values for each individual comparison in the post-hoc analysis (Fig 4A-E).

First, we wondered whether the effects of MT5-MMP variants could occur in the ER, which is the endomembrane system where most protein synthesis occurs. All MT5-MMP variants reduced the levels of HA-C99 in the ER compared with pcDNA (Fig 3F, 4B), suggesting that the presence of MT5-MMP variants induces the exit of HA-C99 toward other cellular compartments. Notably, TM1/IC5 reduced of HA-C99 levels by 17% in the endoplasmic reticulum compared with pcDNA (LogBF10 = 4.68) and induced a greater reduction than TM/IC(ala)EWV (-4%) (LogBF10 = 2.05).

Next, we examined the Golgi apparatus, which is involved in protein packaging and compartmentalization. All MT5-MMP variants induced significant reductions (between 15% and 45%) in HA-C99 compared with pcDNA (Fig 3F, 4C). Among them, TM/IC(ala)EWV was the most common variant, with a particularly significant reduction of 45% and a LogBF10 of 12.89. In addition, HA-C99 reduction in the Golgi was more prominent in TM/IC(ala)EWV (-45%) than in EXT (-16%) (LogBF10 = 2.21), EXT/TM (-17%) (LogBF10 = 0.97), and TM1/IC5 (-15%) (LogBF10 = 1.78). This possibly implies that the presence of MT5-MMP TM associated with an IC structure facilitates HA-C99 translocation outside the Golgi apparatus. A mean reduction of 16% was observed for EXT and TM1/IC5, both lacking the MT5-MMP TM domain, indicating that the presence of MT5-MMP truncated forms reduced HA-C99 in the Golgi apparatus, possibly by inducing rapid entry of HA-C99 into the secretory or endolysosomal pathways.

Co-staining of EEA1 and HA (HA-C99) revealed similar levels of HA-C99 in early endosomes, irrespective of the MT5-MMP construct. However, EXT/TM (+13%) increased HA-C99 translocation into early endosomes compared with pcDNA (LogBF10 = 2.21), TM/IC (LogBF10 = 1.05), and TM5/IC1 (LogBF10 = 1.58) (Fig 3F, 4D). This suggests that MT5-MMP EXT and/or TM, but not MT5-MMP IC, favors the presence of HA-C99 in EEA1+ vesicles. Building upon our previous findings, the levels of co-localization between early endosomes and HA-C99 indicate that EXT/TM preferentially transports HA-C99 from the ER/Golgi toward early endosomes, whereas other MT5-MMP variants may mostly translocate HA-C99 into other cellular compartments.

The dynamics of HA-C99 distribution in lysosomes were similar under different conditions. The two constructs carrying mutations in the intracellular domain, TM/IC(ala)KNKTG and TM/IC(ala)EWV, mainly differed from pcDNA (Fig 3F, 4E), with an increase in HA-C99 colocalization with lysosomes of 18% (LogBF10 = 0.97) and 21% (LogBF10 = 5.27), respectively. Although TM/IC had low LogBF10 values compared with pcDNA (LogBF10 = 0.13), it increased HA-C99 in lysosomes by 18%, which was similar to that of TM/IC(ala)KNKTG and TM/IC(ala)EWV (18% and 21%), which have consistent LogBF10 values. Thus, the presence of MT5-MMP TM and IC (intact or mutated) increases the presence of HA-C99 in lysosomes.

Overall, the expression of certain MT5-MMP constructs modifies HA-C99 distribution in key components of the endomembrane system. All constructs showed a similar trend in promoting a reduction of HA-C99 in the ER and Golgi, while increasing HA-C99 in lysosomes. MT5-MMP TM and IC appeared to play an important role in HA-C99 subcellular sorting, especially in promoting HA-C99 exiting from the Golgi and HA-C99 translocation into lysosomes.

MT5-MMP modifications alter colocalization with HA-C99

On the basis of the aforementioned data, it was unclear whether changes in C99 fate were the consequence of alterations induced by MT5-MMP variants (Fig 5A) in subcellular C99 localization in the endomembrane system or whether these changes underlie proximal interactions between both proteins. To address this issue, we performed a proximity ligation

assay (PLA) using our RPE1 cell-based model[27]. PLA detects when target proteins are within less than 40 nm of each other. Here, HA-C99 and MT5-MMP were targeted using antibodies against the HA and Flag tags present in their N-termini, respectively. For quantitative analysis, we used pcDNA as a normalization control and subtracted the number of positive spots detected in pcDNA from that observed in the MT5-MMP variants. This adjustment was made by considering the number of positive spots in pcDNA as the baseline for nonspecific binding.

Quantification of HA-C99 colocalization differed between all MT5-MMP variants compared with pcDNA. Individually, TM/IC and TM1/IC5 cells had the highest number (25 each) of PLA+ spots per cell (Fig 5B, C). Despite absolute differences, TM/IC variability projects low LogBF10 numbers in individual comparisons with other constructs (Fig 5D). TM1/IC5 (25) increased colocalization with HA-C99 compared with the TM5/IC1 chimera (10) (LogBF10 = 1.56) and EXT (13) (LogBF10 = 1.41). TM/IC(ala)EWV (21) was the third construct with a high number of PLA+ spots, exceeding the 13 spots of EXT (LogBF10 = 0.51) and the 10 of TM5/ICI (LogBF10 = 0.91). Finally, compared with EXT/TM (18), TM5/IC1 (10) showed decreased colocalization with HA-C99 (LogBF10 = 1.17) (Fig 5 A-C). Taken together, our results indicate that the MT5-MMP IC domain plays a role in mediating proteinase colocalization (and eventually interactions) with HA-C99. This role can be challenged by modifications of this domain.

MT5-MMP-based peptides promote C99 degradation

In all cases, selective modifications of the MT5-MMP IC sequence reduced C99 and Aβ accumulation, which is of potential therapeutic interest. We sought to further test this idea by using MT5-MMP IC peptidomimetics containing mutations that efficiently reduced C99 levels when expressed in DNA constructs. We synthesized two peptides, hereafter referred to as p17 and p20. The peptides were co-transfected with HA-C99 in HEK cells and left for 48 h, with no cytotoxic effect revealed by the MTT test (Fig 6A, B). p20 led to a significant 38% decrease in HA-C99 only at the highest concentration of 1000 nM (Fig 6C), while p17 had a dose-response effect at log-scale concentrations of 10, 100 and 1000 nM. The levels of HA-C99 were reduced by 29%, 35%, 53%, and 41%, respectively, which was statistically significant for the last three concentrations (Fig 6D). We selected p17 to be functionalized in a way that

allows entry into cells without the use of transfecting agents. To this end, we conjugated p17 to C5 (C5p17), a VHH (nanobody) that binds to the transmembrane transferrin receptor (TfR), enabling endocytosis and internalization, as previously shown[28]. Transfection of the C5p17 conjugate reduced HA-C99 levels by 37%, 37% and 36% in HEK cells at 1nM, 10 nM and 100 nM, respectively (Fig. 6E), validating the preservation of p17 effects after conjugation.

After western blot confirmation of TfR expression in HEK and RPE1 cells and internalization of C5 in the latter (Fig 6F, G), we conducted free uptake experiments of C5p17 (without transfecting agent) 24 h after transfection of HA-C99. Free uptake of C5p17, as its unconjugated counterpart, had no cytotoxic effects on HEK cells (Fig 6H). The C5p17 conjugate significantly reduced C99 levels by 69% at the 10 nM concentration (Fig 6I).

Overall, our results demonstrate the importance of non-catalytic C-terminal domains of MT5-MMP in the regulation of C99 and Aβ fate, in concert with different degradation pathways. We also highlight the usefulness of leveraging on the molecular plasticity of the C-terminal domains of MT5-MMP to generate molecular tools that help preventing the pathogenic accumulation of C99 and Aβ, and open to the design of peptides with therapeutic potential in the context of AD.

DISCUSSION

In recent years, we have demonstrated the pathological involvement of MT5-MMP in cellular and animal models of AD[13,14,29]. We have also shown the importance of the non-catalytic MT5-MMP domains, in particular the TM and IC, in regulating the metabolism and fate of C99 and Aβ [4]. On this basis, we designed a set of mutations in the TM and IC domains to identify the amino acids responsible for the regulation of APP metabolism and amyloidogenesis by MT5-MMP. We identified key mutations in MT5-MMP residues that affect its interactions with C99 and alter its intracellular distribution and processing. Chimeric combinations of MT5-MMP and MT1-MMP TM and IC unmasked potential differences in C99 affinity and subcellular distribution between MT5-MMP TM and IC when acting separately, ultimately leading to different outcomes for C99 and Aβ accumulation. In addition, KNKTG and PVQ ala substitutions in the IC domain most effectively reduced C99 levels. However, only KNKTG substitutions concordantly reduced Aβ accumulation. Based on these results, we generated and vectorized synthetic peptides of the IC domain carrying these mutations. Only peptides with the KNKTG substitutions decreased C99 levels, reproducing the effect of the mutated DNA plasmids. Overall, the present study identified specific sets of amino acids in the TM and IC domains of MT5-MMP that play a prominent role in controlling C99 fate, opening up new opportunities to exploit MT5-MMP properties to design anti-C99/Aβ therapeutic agents.

Modifications in MT5-MMP domains alter the fate of C99

We previously demonstrated that overexpression of MT5-MMP TM/IC in HEK cells had the same effects on C99 accumulation as full-length MT5-MMP. In contrast, overexpression of MT5-MMP without TM/IC or IC significantly reduced C99 and Aβ levels, highlighting the importance of the C-terminal domains of MT5-MMP in controlling C99/Aβ metabolism[4]. Catalytic inactivation of MT5-MMP EXT (ΔEXT) did not prevent the decrease in C99 levels (mainly through proteasome activity) but restored Aβ levels. This suggests that MT5-MMP proteolytic activity was not involved in C99 degradation, but it might influence Aβ metabolism, as reported for MT1-MMP, which is a close homolog of MT5-MMP[4,30,31]. The lack of Aβ clearance after MT5-MMP EXT inactivation may reflect the ability MT5-MMP EXT to cleave

Aβ in a context of C99 accumulation. Consistent with this idea, incubation of the MT5-MMP catalytic domain and soluble Aβ in a cell-free system truncates the first 4 amino acids of Aβ (unpublished). C99 levels were minimally recovered by inhibition of the autophagolysome system but not of γ-secretase or cathepsin B, suggesting that other processing pathways may play a role in Aβ modulation.

MT1-MMP and MT5-MMP share 60% homology overall, but only ~20% for the TM and IC domains[32], possibly accounting for the opposite effects of MT5-MMP or MT1-MMP variants lacking the IC domain, which respectively decrease and increase C99 levels in HEK cells[4]. Accordingly, chimeric combinations of the TM and IC domains of both MMPs distinctly regulate C99 and Aβ levels. The lack of C99 degradation in the presence of TM5/IC1 suggests that, unlike the TM of MT1-MMP, the TM of MT5-MMP stabilizes C99 by preventing its interaction with proteasomal enzymes or γ-secretase. The lack of effect of LACT or D6 on C99 levels in HEK cells expressing TM5/IC1 supports this hypothesis. In contrast, LACT and D6 rescue C99 levels in TM1/IC5-expressing cells, indicating that the IC of MT5-MMP facilitates C99 processing. It is therefore plausible that the TM of MT5-MMP stabilizes C99, whereas the IC favors its processing, eventually influencing C99 accumulation and Aβ production.

Mutations of specific amino acids of the MT5-MMP IC prevent C99 and Aβ accumulation

Based on the sequence divergence between MT5-MMP and MT1-MMP, we deleted or substituted several amino acid groups in the MT5-MMP IC domain. Deletions barely had any effect, except KNKTG, which significantly decreased C99 levels. This feature was replicated and amplified by ala substitutions of KNKTG or PVQ. Interestingly, only KNKTG substitutions reduce also Aβ levels, indicating the prominent role of the first amino acids consecutive to the TM in the control of both C99 accumulation and Aβ production. The failure of LACT and D6 to restore C99 levels in HEK cells expressing TM/IC(ala)KNKTG may imply the existence of C99 degradation pathways alternative to the proteasome or γ-secretase. This clearly contrasts with previous reports in which it was shown that overexpressed C99 was mainly processed by the proteasome[4,33]. Thus, small modifications in the IC sequence are sufficient to significantly alter C99 processing, thereby stressing the importance of MT5-MMP regulation of C99 fate and the remarkable level of molecular plasticity of the IC domain.

Accordingly, ala substitutions in the C-terminal PDZ-binding EWV motif maintained C99 and Aβ levels compared with TM/IC. However, only D6 clearly upregulated C99 levels, demonstrating the predominant role of γ-secretase in C99 processing. In contrast in the TM/IC control group C99 levels were rescued by both LACT and D6. Altering the C-terminal PDZ-binding motif prevents MT5-MMP recycling to the plasma membrane via interactions with mint3, resulting in MT5-MMP accumulation in the TGN[34]. It is noteworthy that mint3 also binds to APP and regulates its intracellular traffic[35,36]. In our case, EWV substitution strongly reduced C99 localization in the Golgi apparatus, possibly indicating increased export of C99 toward other acidic subcellular compartments where γ-secretase is more active[37–39] and can more efficiently convert it into Aβ.

MT5-MMP variants alter the patterns of subcellular localization of C99

Our results imply potential changes in C99 subcellular distribution that could shed light on differences in C99 processing pathways under the influence of specific MT5-MMP variants. In the same vein it has been shown that subcellular localization of C99/APP influences their processing by canonical secretases and regulates Aβ production[40–42].

PCA revealed that MT5-MMP variants influence HA-C99 distribution differently, highlighting the importance of the TM domain and the PDZ-binding motif to understand these changes. Clustering of the data when all the plasmids are taken together, indicates that TM/IC(ala)EWV is the most influential construct in the subcellular localization of HA-C99, as it alters its distribution in the Golgi, endoplasmic reticulum, and lysosomes. In the case of the other MT5-MMP variants, they limit their influence to a single organelle or none. This difference between the EWV mutations and the others reflects the importance of the MT5-MMP EWV motif in the subcellular localization of C99. Apart from mint3, other members of the Mint family also interact with APP metabolites through binding domains, and overexpression of mint1 or its PTB domain decreased Aβ40 secretion through inhibition of γ-secretase cleavage of C99 in HEK cells[43]. It is thus possible that EWV mutations alter C99 trafficking in a manner that prevents its contact with mint proteins and facilitates γ-secretase cleavage.

Individual analysis for each variant and organelle revealed a general trend toward decreased HA-C99 levels. Most variants reduced HA-C99 levels in the ER, the main site of protein synthesis, possibly indicating the stimulation of C99 sorting to other compartments. We discard the possibility that MT5-MMP variants interfere with C99 synthesis because the variants decreasing C99 levels in the ER do not correlate with decreased levels of C99, as shown in our western blots. With respect to the Golgi apparatus, TM/IC(ala)EWV resulted in the greatest reduction in C99 levels (-45%) compared with the other variants. As noted previously, substitution of the PDZ-binding motif in MT5-MMP TM/IC might facilitate its intracellular localization by impeding recycling into the plasma membrane[34]. Similarly, mint3 knockdown in neuroblastoma cells rerouted APP toward the endolysosomal pathway[44]. These data support our hypothesis that EWV mutations facilitate C99 sorting in the Golgi network to cellular compartments where optimal γ-secretase activity would ensure the maintenance of Aβ levels.

MT5-MMP variants did not change the early endosome content of C99 in most cases. The slight significant increase in cells expressing EXT/TM might be related to the absence of the EWV motif. Concordantly, there is an increase in C99 in early endosomes in the presence of TM/IC(ala)EWV, but the variability in the results makes it statistically insignificant. Conducting additional experiments could provide further evidence to support this hypothesis.

Expression of the TM/IC(ala)KNKTG and TM/IC(ala)EWV variants significantly increase C99 in lysosomes. The fact that these variants had opposite effects on C99 and Aβ content, with the former being a depressant and the latter being a stabilizer, suggests changes in C99 intracellular trafficking before it translocates into lysosomes. In this line, it was shown that inhibition of the autophagosome pathway increases the levels of C99 in LAMP1+ lysosomes in human neuroglioma cells, whereas autophagosome activation causes the opposite effect[45]. However, late endosomes-lysosomes are also major sites of C99 conversion in Aβ[39]. It is possible that KNKTG and EWV mutations in MT5-MMP IC distribute C99 into distinct cellular compartments, thereby reaching lysosomes containing different proteases through separate processing pathways. In addition, TM/IC(ala)EWV increase of C99/Aβ in lysosomes could disrupt endolysosomal function, triggering a pathogenic loop where higher levels of these toxic metabolites facilitate the conversion of more C99 into Aβ[46].

We conclude that different MT5-MMP variants critically affect C99 subcellular distribution. Moreover, whole-domain or minimal mutations in MT5-MMP TM and IC distinctly redistribute C99 in the cellular compartments of the endomembrane system, indicating a key role of the C-terminal domains of MT5-MMP in C99 trafficking. Further work in this direction—incorporating other organelle markers and specific detection methods for C99 and Aβ—could help clarifying the exact correlation of patterns in the subcellular distribution of C99 and their effects on C99 and Aβ accumulation.

Mutations in the IC domain of MT5-MMP determine the interactions with HA-C99

PLA analysis provided additional information on proximal interactions between MT5-MMP variants and HA-C99. TM/IC and TM1/IC5—both containing intact MT5-MMP IC—showed the highest level of interaction with HA-C99. Striking differences emerged between the chimeras, with TM5/IC1 exhibiting low levels of PLA+ signaling. This indicates that the IC of MT5-MMP facilitates the colocalization of MT5-MMP and C99, which is consistent with data showing that the TM/IC of MT5-MMP was sufficient to coimmunoprecipitate HA-C99 in HEK cells[4]. The strong reduction in PLA+ signal upon expression of TM5/IC1 or EXT confirms the relevance of MT5-MMP IC for the proximal interaction with C99. However, the increase in EXT/TM colocalization with C99 compared with EXT may indicate that MT5-MMP TM is also important for proximal localization with C99. Together with the decrease in TM5/IC1, these data suggest that the interface between MT5-MMP TM and IC is important but not exclusive in preserving MT5-MMP and C99 proximal interactions. This would explain why mutations in EWV have little effect on proximal interactions with C99 compared with the TM/IC control, whereas KNKTG substitutions tend to decrease the number of colocalizations. These results highlight the importance of the IC domain of MT5-MMP in mediating interactions between MT5-MMP and HA-C99, which are impaired when the domain is widely mutated. Moreover, we can observe a prominent role for MT5-MMP TM when is associated with MT5-MMP domains, which would presumably better preserve its native structure. It will be important to elaborate on the impact of MT5-MMP TM mutations along with small modifications (*e.g.* EWV or KNKTG) of MT5-MMP IC to determine the residues responsible for interactions with C99.

Intracellular delivery of a synthetic MT5-MMP IC peptide mimicking the KNKTG mutation reduces C99 accumulation

Collectively, our results demonstrate that mutated variants of MT5-MMP differentially modulate C99 in heterologous cell lines. Furthermore, we have revealed the fundamental importance of the MT5-MMP IC in determining the fate of C99 through complex molecular mechanisms involving proximity interactions and the translocation of C99 into specific cellular compartments. Thus, we hypothesized that the properties of MT5-MMP non-catalytic domains possess important therapeutic potential. Synthetic peptides imitate natural amino acid structures with specific biological properties and are significant therapeutic tools extensively used[47]. As a proof-of-concept, we generated synthetic peptides mimicking the modified amino acids sequences of MT5-MMP IC that downregulate C99 levels, and vectorized them using a VHH that recognizes the TfR. We tested peptides containing the IC domain with (ala)KNKTG or (ala)PVQ sequences in HEK cells overexpressing C99. A dose-response protocol demonstrated the ability of the peptide incorporating (ala)KNKTG to greatly reduce C99 in live cells, demonstrating that it is possible to use MT5-MMP IC-based therapeutic tools to modulate C99. In this regard, a recent study showed that editing the YENPTY motif of the C99 sequence, which is essential for its trafficking, resulted in a stable reduction of C99 and Aβ levels in an AD knock-in mouse model. This highlights the importance of targeting APP metabolites using strategies that affect their trafficking and eventual production of toxic biofactors[48]. Our study adds to this work by demonstrating the possibility of using MT5-MMP as a reference to generate synthetic peptides, which is a generally safe therapeutic strategy that avoids the use of genome-modifying tools.

Declarations

Ethics approval

All the experimental procedures were conducted in agreement with the authorization by the French Ministry of Research to the laboratory (# 7950), as defined in the directive 2009/41/CE of the European Parliament and the European Council of May 6 2009 for the use of genetically modified organisms.

Availability of data and materials

All the data generated or analyzed during this study are included in this published article and are available from the corresponding author upon reasonable request.

All the analysis files in the form of Jupyter Notebook are uploaded and freely accessible at: github.com/RiveraLabINP/BelioMairal_2024

Competing interests

MK was director of the Institute of Neuropathophysiology, UMR7051 academic neuroscience laboratory supported by the CNRS and Aix-Marseille University, but also co-founder, shareholder and scientific counsel of the VECT-HORUS biotechnology company. The other authors declare that they have no competing interests.

Funding

This work was supported by funding from the CNRS and Aix-Marseille Université and by public grants to overseen by "Fondation pour la Recherche Médicale" (FRM), by the French National Agency for Research (ANR) MT5-AD and Fondation Vaincre Alzheimer to SR. PB received a doctoral fellowship from the French government under the Programme Investissements d'Avenir, Initiative d'Excellence d'Aix-Marseille Université via A*Midex (AMX-19-IET-004) and ANR (ANR-17-EURE-0029) funding through NeuroSchool/NeuroMarseille. AK received an international mobility grant under the same program. PB also received financial support from Fondation Vaincre Alzheimer.

REFERENCES

1. Rivera S, Khrestchatisky M, Kaczmarek L, Rosenberg GA, Jaworski DM. Metzincin proteases and their inhibitors: foes or friends in nervous system physiology? *J Neurosci*. 2010;30(46):15337-15357. doi:10.1523/JNEUROSCI.3467-10.2010

2. Sekine-Aizawa Y, Hama E, Watanabe K, et al. Matrix metalloproteinase (MMP) system in brain: identification and characterization of brain-specific MMP highly expressed in cerebellum: MT5-MMP: a brain-specific MMP in rat. *European Journal of Neuroscience*. 2001;13(5):935-948. doi:10.1046/j.0953-816x.2001.01462.x

3. Jaworski DM. Developmental regulation of membrane type-5 matrix metalloproteinase (MT5-MMP) expression in the rat nervous system. *Brain research*. 2000;860(1-2):174-177.

4. García-González L, Paumier J, Louis L, et al. MT5-MMP controls APP and β-CTF/C99 metabolism through proteolytic-dependent and -independent mechanisms relevant for Alzheimer's disease. *FASEB j*. 2021;35(7). doi:10.1096/fj.202100593R

5. Rivera S, García-González L, Khrestchatisky M, Baranger K. Metalloproteinases and their tissue inhibitors in Alzheimer's disease and other neurodegenerative disorders. *Cell Mol Life Sci*. 2019;76(16):3167-3191. doi:10.1007/s00018-019-03178-2

6. Monea S, Jordan BA, Srivastava S, DeSouza S, Ziff EB. Membrane Localization of Membrane Type 5 Matrix Metalloproteinase by AMPA Receptor Binding Protein and Cleavage of Cadherins. *J Neurosci*. 2006;26(8):2300-2312. doi:10.1523/JNEUROSCI.3521-05.2006

7. Porlan E, Martí-Prado B, Morante-Redolat JM, et al. MT5-MMP regulates adult neural stem cell functional quiescence through the cleavage of N-cadherin. *Nat Cell Biol*. 2014;16(7):629-638. doi:10.1038/ncb2993

8. Warren KM, Reeves TM, Phillips LL. MT5-MMP, ADAM-10, and N-cadherin act in concert to facilitate synapse reorganization after traumatic brain injury. *J Neurotrauma*. 2012;29(10):1922-1940. doi:10.1089/neu.2012.2383

9. Komori K, Nonaka T, Okada A, et al. Absence of mechanical allodynia and Aβ-fiber sprouting after sciatic nerve injury in mice lacking membrane-type 5 matrix metalloproteinase. *FEBS Letters*. 2004;557(1-3):125-128. doi:10.1016/S0014-5793(03)01458-3

10. Ahmad M, Takino T, Miyamori H, Yoshizaki T, Furukawa M, Sato H. Cleavage of amyloid-beta precursor protein (APP) by membrane-type matrix metalloproteinases. *J Biochem*. 2006;139(3):517-526. doi:10.1093/jb/mvj054

11. Willem M, Tahirovic S, Busche MA, et al. η-Secretase processing of APP inhibits neuronal activity in the hippocampus. *Nature*. 2015;526(7573):443-447. doi:10.1038/nature14864

12. Selkoe DJ, Hardy J. The amyloid hypothesis of Alzheimer's disease at 25 years. *EMBO Mol Med*. 2016;8(6):595-608. doi:10.15252/emmm.201606210

13. Baranger K, Marchalant Y, Bonnet AE, et al. MT5-MMP is a new pro-amyloidogenic proteinase that promotes amyloid pathology and cognitive decline in a transgenic mouse model of Alzheimer's disease. *Cell Mol Life Sci*. 2016;73(1):217-236. doi:10.1007/s00018-015-1992-1

14. Baranger K, Bonnet AE, Girard SD, et al. MT5-MMP Promotes Alzheimer's Pathogenesis in the Frontal Cortex of 5xFAD Mice and APP Trafficking in vitro. *Front Mol Neurosci*. 2017;9. doi:10.3389/fnmol.2016.00163

15. Mensch M, Dunot J, Yishan SM, et al. Aη-α and Aη-β peptides impair LTP ex vivo within the low nanomolar range and impact neuronal activity in vivo. *Alzheimer's Research & Therapy*. 2021;13(1):125. doi:10.1186/s13195-021-00860-1

16. Afram E, Lauritzen I, Bourgeois A, et al. The η-secretase-derived APP fragment ηCTF is localized in Golgi, endosomes and extracellular vesicles and contributes to Aβ production. *Cell Mol Life Sci*. 2023;80(4):97. doi:10.1007/s00018-023-04737-4

17. Lauritzen I, Pardossi-Piquard R, Bauer C, et al. The -Secretase-Derived C-Terminal Fragment of APP, C99, But Not A , Is a Key Contributor to Early Intraneuronal Lesions in Triple-Transgenic Mouse Hippocampus. *Journal of Neuroscience*. 2012;32(46):16243-16255. doi:10.1523/JNEUROSCI.2775-12.2012

18. Py NA, Bonnet AE, Bernard A, et al. Differential spatio-temporal regulation of MMPs in the 5xFAD mouse model of Alzheimerâ€^{TM}s disease: evidence for a pro-amyloidogenic role of MT1-MMP. *Front Aging Neurosci*. 2014;6. doi:10.3389/fnagi.2014.00247

19. Pulina MV, Hopkins M, Haroutunian V, Greengard P, Bustos V. C99 selectively accumulates in vulnerable neurons in Alzheimer's disease. *Alzheimer's & Dementia*. 2020;16(2):273-282. doi:10.1016/j.jalz.2019.09.002

20. Kwart D, Gregg A, Scheckel C, et al. A Large Panel of Isogenic APP and PSEN1 Mutant Human iPSC Neurons Reveals Shared Endosomal Abnormalities Mediated by APP β-CTFs, Not Aβ. *Neuron*. 2019;104(2):256-270.e5. doi:10.1016/j.neuron.2019.07.010

21. Schindelin J, Arganda-Carreras I, Frise E, et al. Fiji: an open-source platform for biological-image analysis. *Nat Methods*. 2012;9(7):676-682. doi:10.1038/nmeth.2019

22. Bowman EJ, Siebers A, Altendorf K. Bafilomycins: a class of inhibitors of membrane ATPases from microorganisms, animal cells, and plant cells. *Proceedings of the National Academy of Sciences*. 1988;85(21):7972-7976. doi:10.1073/pnas.85.21.7972

23. Mueller-Steiner S, Zhou Y, Arai H, et al. Antiamyloidogenic and neuroprotective functions of cathepsin B: implications for Alzheimer's disease. *Neuron*. 2006;51(6):703-714. doi:10.1016/j.neuron.2006.07.027

24. Asai M, Yagishita S, Iwata N, Saido TC, Ishiura S, Maruyama K. An alternative metabolic pathway of amyloid precursor protein C-terminal fragments via cathepsin B in a human neuroglioma model. *FASEB J*. 2011;25(10):3720-3730. doi:10.1096/fj.11-182154

25. Klimanskaya I. Retinal Pigment Epithelium. In: *Methods in Enzymology*. Vol 418. Embryonic Stem Cells. Academic Press; 2006:169-194. doi:10.1016/S0076-6879(06)18011-8

26. Keysers C, Gazzola V, Wagenmakers EJ. Using Bayes factor hypothesis testing in neuroscience to establish evidence of absence. *Nat Neurosci*. 2020;23(7):788-799. doi:10.1038/s41593-020-0660-4

27. Söderberg O, Gullberg M, Jarvius M, et al. Direct observation of individual endogenous protein complexes in situ by proximity ligation. *Nat Methods*. 2006;3(12):995-1000. doi:10.1038/nmeth947

28. COHEN R, David M, Khrestchatisky M. Transferrin receptor-binding molecules, conjugates thereof and their uses. Published online July 16, 2020. Accessed July 8, 2024. https://patents.google.com/patent/WO2020144233A1/en

29. Pilat D, Paumier JM, García-González L, et al. MT5-MMP promotes neuroinflammation, neuronal excitability and Aβ production in primary neuron/astrocyte cultures from the 5xFAD mouse model of Alzheimer's disease. *J Neuroinflammation*. 2022;19(1):65. doi:10.1186/s12974-022-02407-z

30. García-González L, Pilat D, Baranger K, Rivera S. Emerging Alternative Proteinases in APP Metabolism and Alzheimer's Disease Pathogenesis: A Focus on MT1-MMP and MT5-MMP. *Front Aging Neurosci*. 2019;11:244. doi:10.3389/fnagi.2019.00244

31. Paumier JM, Py NA, García-González L, et al. Proamyloidogenic effects of membrane type 1 matrix metalloproteinase involve MMP-2 and BACE-1 activities, and the modulation of APP trafficking. *FASEB j*. 2019;33(2):2910-2927. doi:10.1096/fj.201801076R

32. Pei D. Identification and Characterization of the Fifth Membrane-type Matrix Metalloproteinase MT5-MMP *. *Journal of Biological Chemistry*. 1999;274(13):8925-8932. doi:10.1074/jbc.274.13.8925

33. Evrard C, Kienlen-Campard P, Coevoet M, et al. Contribution of the Endosomal-Lysosomal and Proteasomal Systems in Amyloid-β Precursor Protein Derived Fragments Processing. *Front Cell Neurosci*. 2018;12:435. doi:10.3389/fncel.2018.00435

34. Wang P, Wang X, Pei D. Mint-3 Regulates the Retrieval of the Internalized Membrane-type Matrix Metalloproteinase, MT5-MMP, to the Plasma Membrane by Binding to Its Carboxyl End Motif EWV *. *Journal of Biological Chemistry*. 2004;279(19):20461-20470. doi:10.1074/jbc.M400264200

35. Caster AH, Kahn RA. Recruitment of the Mint3 Adaptor Is Necessary for Export of the Amyloid Precursor Protein (APP) from the Golgi Complex. *Journal of Biological Chemistry*. 2013;288(40):28567-28580. doi:10.1074/jbc.M113.481101

36. Ho A, Liu X, Südhof TC. Deletion of Mint proteins decreases amyloid production in transgenic mouse models of Alzheimer's disease. *J Neurosci*. 2008;28(53):14392-14400. doi:10.1523/JNEUROSCI.2481-08.2008

37. Cai T, Hatano A, Kanatsu K, Tomita T. Histidine 131 in presenilin 1 is the pH-sensitive residue that causes the increase in Aβ42 level in acidic pH. *J Biochem*. 2020;167(5):463-471. doi:10.1093/jb/mvz110

38. Kanatsu K, Hori Y, Ebinuma I, Chiu YW, Tomita T. Retrograde transport of γ-secretase from endosomes to the trans-Golgi network regulates Aβ42 production. *Journal of Neurochemistry*. 2018;147(1):110-123. doi:10.1111/jnc.14477

39. Maesako M, Houser MCQ, Turchyna Y, Wolfe MS, Berezovska O. Presenilin/γ-Secretase Activity Is Located in Acidic Compartments of Live Neurons. *J Neurosci*. 2022;42(1):145-154. doi:10.1523/JNEUROSCI.1698-21.2021

40. Choy RWY, Cheng Z, Schekman R. Amyloid precursor protein (APP) traffics from the cell surface via endosomes for amyloid β (Aβ) production in the trans-Golgi network. *Proceedings of the National Academy of Sciences*. 2012;109(30):E2077-E2082. doi:10.1073/pnas.1208635109

41. Roselli S, Satir TM, Camacho R, et al. APP-BACE1 Interaction and Intracellular Localization Regulate Aβ Production in iPSC-Derived Cortical Neurons. *Cell Mol Neurobiol*. 2023;43(7):3653-3668. doi:10.1007/s10571-023-01374-0

42. Wang J, Gleeson PA, Fourriere L. Spatial-Temporal Mapping Reveals the Golgi as the Major Processing Site for the Pathogenic Swedish APP Mutation: Familial APP Mutant Shifts the Major APP Processing Site. *Traffic*. 2024;25(3):e12932. doi:10.1111/tra.12932

43. King GD, Cherian K, Turner RS. X11alpha impairs gamma- but not beta-cleavage of amyloid precursor protein. *J Neurochem*. 2004;88(4):971-982. doi:10.1046/j.1471-4159.2003.02234.x

44. Shrivastava-Ranjan P, Faundez V, Fang G, et al. Mint3/X11gamma is an ADP-ribosylation factor-dependent adaptor that regulates the traffic of the Alzheimer's Precursor protein from the trans-Golgi network. *Mol Biol Cell*. 2008;19(1):51-64. doi:10.1091/mbc.e07-05-0465

45. González AE, Muñoz VC, Cavieres VA, et al. Autophagosomes cooperate in the degradation of intracellular C-terminal fragments of the amyloid precursor protein via the MVB/lysosomal pathway. *FASEB J*. 2017;31(6):2446-2459. doi:10.1096/fj.201600713R

46. Bretou M, Sannerud R, Escamilla-Ayala A, et al. Accumulation of APP C-terminal fragments causes endolysosomal dysfunction through the dysregulation of late endosome

to lysosome-ER contact sites. *Dev Cell*. 2024;59(12):1571-1592.e9. doi:10.1016/j.devcel.2024.03.030

47. Vlieghe P, Lisowski V, Martinez J, Khrestchatisky M. Synthetic therapeutic peptides: science and market. *Drug Discov Today*. 2010;15(1-2):40-56. doi:10.1016/j.drudis.2009.10.009

48. Aulston BD, Gimse K, Bazick HO, et al. Long term rescue of Alzheimer's deficits in vivo by one-time gene-editing of App C-terminus. *bioRxiv*. Published online June 9, 2024:2024.06.08.598099. doi:10.1101/2024.06.08.598099

LEGENDS

Table 1. List of inhibitors. Provides a list of the inhibitors, at which stock concentration they were resuspended, at which dilution they were used, and the references.

Table 2. List of antibodies. Provides a list of the targets of the antibodies used, the host where they were produced, the working dilution, the references, and the application they were used for. PLA refers to proximity ligation assay.

Figure 1. Whole-domain modifications modulate the accumulation of C99 and the production of Aβ in HEK cells.

(A) Schematic view of different constructs generated from the MT5-MMP sequence. (B) Graph representing the absence of cytotoxicity in HEK cells measured by the MTT test 48 h after co-transfection of HEK cells with C99 and different MT5-MMP variants. Absorbance values at 450-10 nm are represented in arbitrary units (A.U) and normalized to those of samples treated only with the transfection reagent. (C) Representative western blots of HEK cells overexpressing C99 with TM/IC, EXT, EXT/TM, or ΔEXT. C99 was detected using a rabbit anti-APP-CTF antibody. The graph on the right represents the semi-quantifications of C99 levels normalized with actin as the protein load control and with pcDNA conditions to normalize each independent experiment. (D) Graphical representation of Aβ40 concentrations in the supernatants of HEK cells overexpressing C99 with TM/IC, EXT, EXT/TM, or ΔEXT. The values of each independent experiment were normalized to the pcDNA condition to control for inter-experimental variability. (E) Representative western blots of HEK cells overexpressing C99 with TM/IC, EXT, EXT/TM, TM5/IC1, or TM1/IC5. C99 was detected using a rabbit anti-APP-CTF antibody. The graph on the right represents semi-quantifications of C99 levels normalized using actin as a protein load control and with pcDNA condition to normalize each independent experiment. (F) Graphical representation of the concentrations of Aβ40 in the supernatants of HEK cells overexpressing C99 with TM/IC, EXT, EXT/TM, TM5/IC1, or TM1/IC5. The values of each independent experiment were normalized with the pcDNA condition to control for inter-experimental variability. (G-J) Representative western

blots of HEK cells overexpressing C99 with (G) EXT, (H) ΔEXT, (I) TM5/IC1 or (J) TM1/IC5 variants, and the corresponding actin-normalized quantifications below each immunoblots. Cells were treated for 20 h with inhibitors of the C99 processing pathways: proteasome (lactacystin; LACT 10 μM); γ-secretase ELND006 (D6 1 μM); cathepsin (B CA-074 Me; CA074 10 μM); and autophagolysosomal pathway (bafilomycin A1; BAFA 50 nM). DMSO was used as control. C99 was detected using a rabbit anti-APP-CTF antibody. All statistical tests were ANOVA with Dunnett's post hoc multiple comparison test compared with the control condition, with at least three independent experiments. Values are presented as mean ± SEM. P-values are represented as * $p < 0.05$, ** $p < 0.01$, *** $p < 0.001$, and **** $p < 0.0001$.

Fig 2. Mutation of specific MT5-MMP IC residues decreases C99 and Aβ levels in HEK cells.

(A) Schematic view of different constructs generated from the MT5-MMP sequence. The amino acid groups in red were either deleted or substituted with ala. These groups were: KNKTG, QPVT, YK, PVQ, and EWV. (B) Graph representing the absence of cytotoxicity in HEK cells measured by the MTT test 48 h after cotransfection of HEK cells with C99 and different MT5-MMP variants. Absorbance values at 450-10 nm are represented in arbitrary units (A.U) and normalized to those of samples treated only with the transfection reagent. (C) Representative western blots of HEK cells overexpressing C99 with TM/IC or TM/IC with deletions in KNKTG, QPVT, YK, PVQ or EWV. C99 was detected using a rabbit anti-APP-CTF antibody. The graph below represents the semi-quantifications of C99 levels normalized with actin as the protein load control and with pcDNA conditions to normalize each independent experiment. (D) Representative western blot of HEK cells overexpressing C99 with TM/IC or TM/IC with ala substitutions in KNKTG, QPVT, YK, PVQ, EWV or all the targeted groups (All). C99 was detected using a rabbit anti-APP-CTF antibody. The graph below represents the semi-quantifications of C99 levels normalized with actin as the protein load control and with pcDNA conditions to normalize each independent experiment. (E) Graphical representation of Aβ40 concentrations in the supernatants of HEK cells overexpressing C99 with mutations in the IC that reduce C99 levels or that maintain similar pathologic C99 levels to TM/IC control; these were TM/IC, TM/IC(ala)KNKTG, TM/IC(ala)PVQ, TM/IC(ala)EWV or TM/IC(ala)All. The values of each independent experiment were normalized with the pcDNA condition to control for inter-experimental

variability. (F-H) Representative western blots of HEK cells overexpressing C99 with (F) TM/IC, (G) TM/IC(ala)KNKTG, or (H) TM/IC(ala)EWV treated for 20 h with inhibitors of the C99 processing pathways: Proteasome lactacystin (LACT 10 μM); γ-secretase (ELND006; D6 1μM). All inhibitors were resuspended in DMSO at a final 1:5000 concentration. DMSO 1:5000 was used as control. C99 was detected using a rabbit anti-APP-CTF antibody. The graphs represent semi-quantification of C99 levels in western blots normalized to actin as a protein load control. All statistical tests were ANOVA with Dunnett's post hoc multiple comparison test compared with the control condition, with at least three independent experiments. Values are presented as mean ± SEM. P-values are represented as * $p < 0.05$, ** $p < 0.01$, *** $p < 0.001$, and **** $p < 0.0001$.

Fig 3. Effect of MT5-MMP IC domain residue modification on C99 subcellular distribution in RPE1 cells.

(A) Schematic view of different constructs generated from the MT5-MMP sequence. The amino acids in red represent the targeted groups that were substituted with ala. These groups were: KNKTG and EWV. (B) Western blotting demonstrating the lack of MT5-MMP expression in lysates of both HEK and RPE1 cells. (C) Heatmap representing the quantification of the area of HA+ signal overlapping with each organelle from the endomembrane system of RPE1 cells, depending on the MT5-MMP variant co-transfected with HA-C99. The values represent the percentage change in the area of overlap relative to that of pcDNA. The values that represent a decrease in the area of overlap of HA/organelle are blue and darker, whereas higher values are represented in green and lighter colors. For instance, TM/IC(ala)EWV in Golgi is represented in dark color because its area of overlap with HA/Golgi is -45% of that in pcDNA. On the contrary, there was an increase of +21% in the overlap area of HA/lysosomes in TM/IC(ala)EWV; thus, the color was light green. (D) PCA of the quantification heatmap in (C) constructed with two components representing 75% of the total variability of the data. Each MT5-MMP variant clustered with variants that had similar profiles of change with respect to pcDNA in the overlap area of HA and different endomembrane organelles. This indicates that pcDNA and TM/IC(ala)EWV are the two most different conditions compared with the other MT5-MMP variants. In contrast, EXT and TM1/IC5 cluster together, indicating similar changes in HA distribution through the endomembrane system compared with pcDNA. (E)

Cluster map representing changes in (C) based on Bayesian ANOVA. The values in the cluster map are the summed LogBF10 values of multiple comparisons between different MT5-MMP variants in each organelle, which represent the statistical strength of variability in HA overlap with organelles for each MT5-MMP variant. High values indicate stronger statistical evidence of changes in HA overlap in a given MT5-MMP variant with respect to all other variants within the same organelle. The lower the values are, the stronger is the evidence that the MT5-MMP variant does not induce changes in HA overlap within a specific organelle compared with all other MT5-MMP variants. Higher values are represented in light-to-darker red, and lower values are represented in light-to-darker blue. In this cluster map, one can understand that TM/IC(ala)EWV particularly affects HA overlap in the Golgi, ER, and lysosomes compared with all other MT5-MMP variants; and TM1/IC5 specifically affects HA signal overlap with the ER. However, compared with the other variants, EXT did not alter the HA overlap with lysosomes compared to the other variants. (F) Representative images of HA signal overlapping with immunolabelling for either early endosomes or Golgi or ER or lysosomes in RPE1 co-transfected with HA-C99 and the MT5-MMP variants used in this experiment and represented in (A). The organelles are represented in magenta, and the HA signal is represented in cyan. The multiline plots represent the fluorescence intensity distribution along the 20 μm of yellow line in the image. The scale bar represents 10 μm.

Fig 4. LogBF10 values of individual differences in HA-C99 subcellular localization in specific subcellular compartments within RPE1 cells transfected with distinct MT5-MMP variants.

(A) Schematic view of different constructs generated from the MT5-MMP sequence. The amino acids in red represent the targeted groups that were substituted with ala. These groups were: KNKTG and EWV. (B-E) The diagonal correlation matrices represent the LogBF10 values for each comparison within a Bayesian ANOVA, with post-hoc multiple comparison of the percentage of change in HA overlap with respect to pcDNA between different MT5-MMP variants; the ER (B), the Golgi (C), early endosomes (D), and lysosomes (E). Higher values are represented in light-to-darker red, and lower values are represented in light-to-darker blue. Next to each MT5-MMP variant is a color representation of the quantitative value of the area of overlap of HA and organelle previously shown in a heatmap (Fig 3C) to facilitate

interpretation of the LogBF10 values. As before, the values that represent a decrease in the area of HA/organelle overlap are blue and darker, whereas higher values are represented in green and lighter colors. Therefore, in (C) Golgi, the LogBF10 value in the comparison between TM/IC(ala)EWV and pcDNA indicates that statistical analysis strongly supports the presence of a difference in HA overlap with that observed in Golgi. Values close to 0 indicate that there is not enough evidence to determine whether there is a difference. Negative values describe strong evidence supporting the finding of no difference in the comparison of means.

Fig 5. Altering the MT5-MMP IC domain residues disrupts interactions with C99.

(A) Schematic view of different constructs generated from the MT5-MMP sequence. The amino acids in red represent the targeted groups that were substituted with ala. These groups were: KNKTG and EWV. (B) Representative images of the Operetta© HCS imaging results of PLA in RPE1 cells co-transfected with HA-C99 and various MT5-MMP variants described in (A). The orange dots correspond to PLA+ spots that translate the proximity of HA (HA-C99) and Flag (MT5-MMP variant) to less than 40 nm. Rat anti-HA and rabbit anti-Flag antibodies were used to tag the HA-C99 and MT5-MMP variants, respectively. The goat anti-rat and goat anti-rabbit conjugated to DuoLink© orange oligos were used as secondary antibodies for later ligation, amplification, and detection. The representative images show segmented cells defining the nucleus and plasma membrane. The scale bar represents 10 μm. (C) Quantification of PLA+ spots in each MT5-MMP variant. PLA+ spots in pcDNA were subtracted from the other conditions, as we considered them to represent the baseline unspecific signal. The values representing a small number of PLA+ spots are blue and darker, whereas higher PLA+ spots are represented in green and lighter colors. Here, TM/IC represents 25 PLA+ spots per cell (light green color). In contrast, pcDNA represents 0 PLA+ spots per cell; thus, it is darkly colored. (D) The diagonal correlation matrix represents the LogBF10 values for each comparison in a Bayesian ANOVA with post-hoc multiple comparisons of the number of PLA+ spots between different MT5-MMP variants. Higher values are represented in light-to-darker red, and lower values are represented in light-to-darker blue. For instance, the difference in PLA+ spots between TM1/IC5 and TM5/IC1 has a LogBF10 value of 1.56, which suggests that one can assume there is a difference in the mean number of PLA+ spots per cell between these two variants.

Figure 6. Effects of modified peptides of the MT5-MMP IC domain on C99 levels in heterologous cell lines.

(A-B) Amino acid sequence of the (A) p20 and (B) p17, corresponding to MT5-MMP IC with PVQ and KNKTG substituted with ala groups (in red), respectively. Graph representing the absence of cytotoxicity in HEK cells measured by the MTT test 48 h after cotransfection with C99 and p20 (A) or p17 (B). Absorbance values at 450-10 nm are represented in arbitrary units (A.U) and normalized to those of samples treated only with the transfection reagent. (C-E) Representative western blots of HEK cells overexpressing HA-C99 co-transfected with the peptides p20 (C), p17 (D) or conjugated p17 (C5p17) (E) at log-scaled concentrations from 0 to 1000 nM. HA-C99 was detected using a rat anti-HA antibody. The graphs represent semi-quantifications of HA-C99 levels normalized to actin as the protein load control. (F) Representative confocal images of RPE1 cells demonstrating that our TfR antibody specifically detects human TfR in human cells. (G) Western blot of TfR in HEK and RPE1 cell lysates, showing expression of TfR in both cell types. (H) As in (A-B), the graph represents the absence of cytotoxicity in HEK cells measured by the MTT test 48 h after transfection with HA-C99 and subsequent treatment with C5p17. (I) Sequence representing the VHH C5 conjugated to p17. Below is a representative image of a western blot of HEK cell lysates transfected with HA-C99 and incubated for 48 h with C5p17 at concentrations log-scaled from 0 to 1000 nM. HA-C99 was detected using a rat anti-HA antibody. The graph represents semi-quantifications of HA-C99 levels normalized to actin as the protein load control. All statistical tests were ANOVA with Dunnett's post hoc multiple comparison test compared with the control condition, with at least three independent experiments. Values are presented as mean ± SEM. P-values are represented as * $p < 0.05$, ** $p < 0.01$, *** $p < 0.001$, and **** $p < 0.0001$.

TABLES

Table 1

Inhibitors				
Inhibitor	**[Stock](µM)**	**Dilution**	**Reference**	**Company**
LACT	**10**	**1:5000**	**BML-PI104-1000**	**Enzo Life Sciences**
D6	**1**	**1:5000**	**SML2122**	**Sigma-Aldrich**
BAFA1	**250**	**1:5000**	**B1793**	**Sigma-Aldrich**
CA074	**50000**	**1:5000**	**205531**	**Sigma-Aldrich**

Table 2

Antibodies					
Target	**Host**	**Dilution**	**Reference**	**Company**	**Application**
Primaries					
APP-CTF	**Rabbit**	**1:1000**	**A8717**	**Sigma-Aldrich**	**Western blot**
Actin	**Mouse**	**1:5000**	**A1978**	**Sigma-Aldrich**	**Western blot**
TfR1	**Rabbit**	**1:1000 1:300**	**GTX102596**	**GeneTex**	**Western blot Immunofluorescence**
Nogo-B	**Sheep**	**1:25**	**AF6034**	**Biotechne**	**Immunofluorescence**
GM130	**Mouse**	**1:200**	**610823**	**BD Biosciences**	**Immunofluorescence**
EEA1	**Mouse**	**1:100**	**sc-365652**	**Santa Cruz Biotechnology**	**Immunofluorescence**
LAMP1	**Rabbit**	**1:300**	**ab24170**	**Abcam**	**Immunofluorescence**
HA	**Rat**	**1:100 1:100**	**11867423001**	**Roche**	**Immunofluorescence PLA**
Flag	**Rabbit**	**1:200**	**14793**	**Cell Signaling Technology**	**PLA**
Secondaries					
Rabbit	**Goat**	**1:800**	**111-005-003**	**Jackson ImmunoResearch**	**PLA**
Rat	**Goat**	**1:800**	**112-005-003**	**Jackson ImmunoResearch**	**PLA**
Mouse-647	**Donkey**	**1:800**	**A32787**	**ThermoFisher Scientific**	**Immunofluorescence**
Rabbit-647	**Donkey**	**1:800**	**A32795**	**ThermoFisher Scientific**	**Immunofluorescence**
Sheep-647	**Donkey**	**1:800**	**A21448**	**ThermoFisher Scientific**	**Immunofluorescence**
Rat-488	**Donkey**	**1:800**	**A48269**	**ThermoFisher Scientific**	**Immunofluorescence**
Rabbit-488	**Donkey**	**1:800**	**A-21206**	**ThermoFisher Scientific**	**Immunofluorescence**
Mouse-594	**Donkey**	**1:800**	**A-21203**	**ThermoFisher Scientific**	**Immunofluorescence**

FIGURES

Fig 1

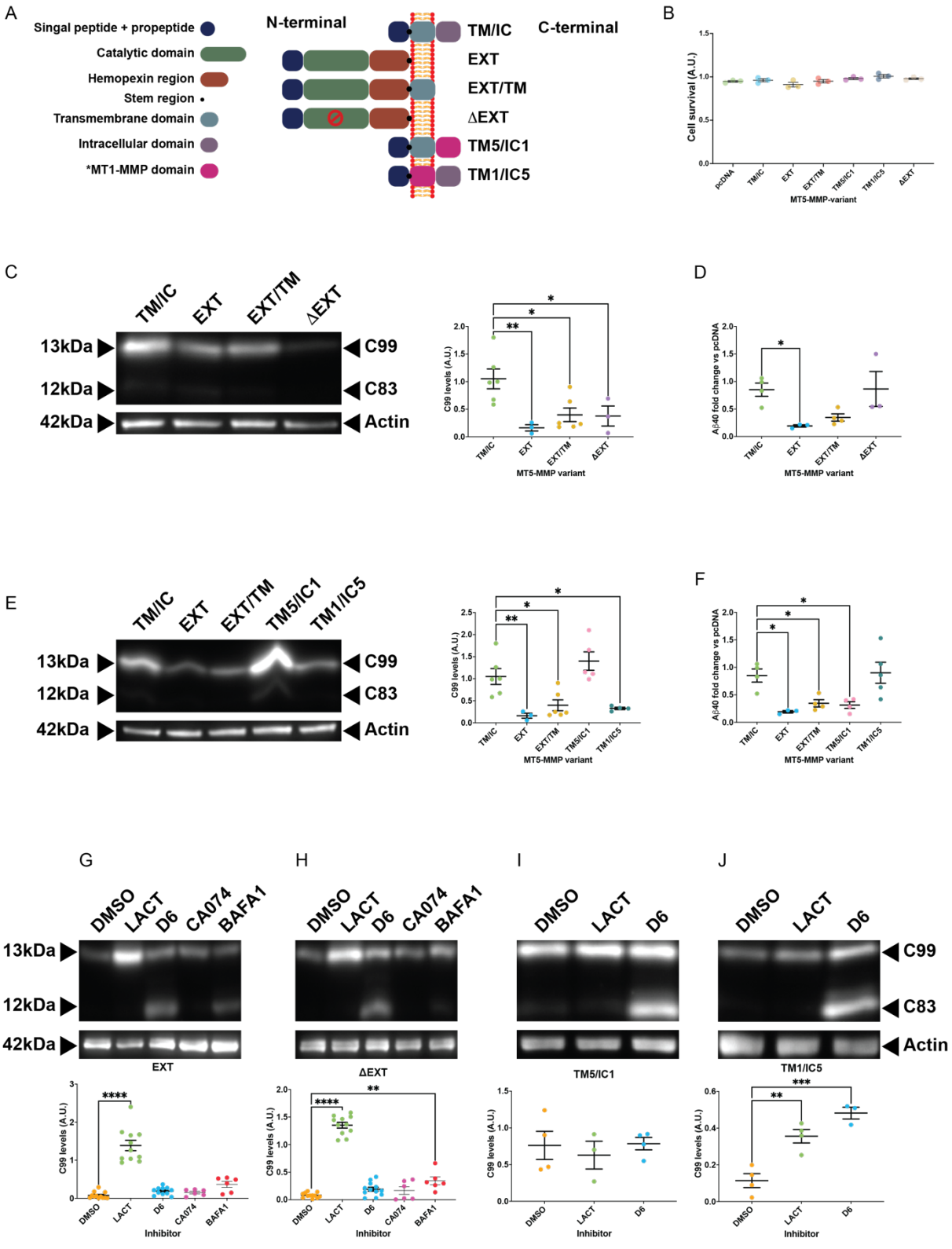

Fig 2.

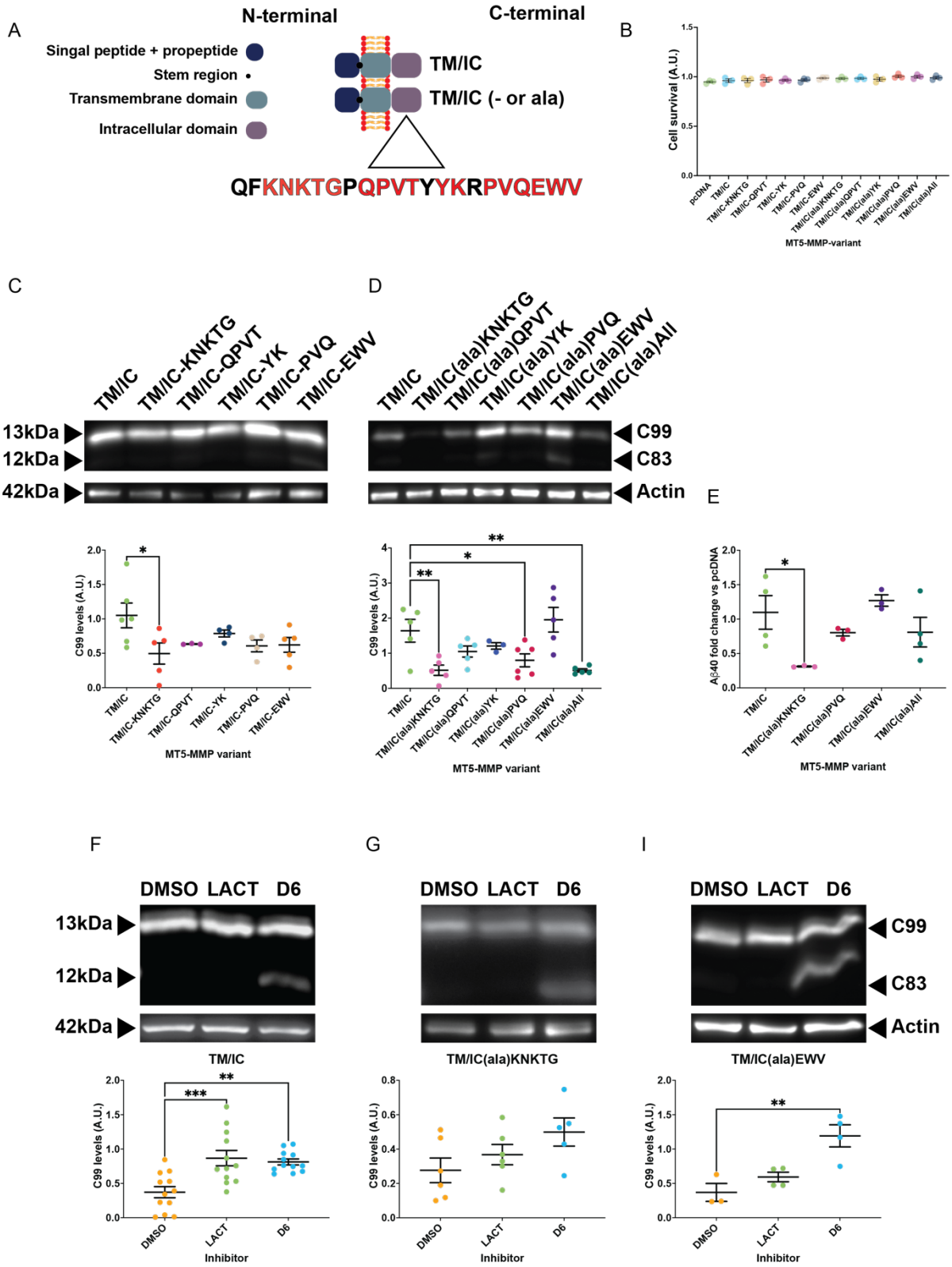
A
N-terminal
C-terminal
Singal peptide + propeptide
Stem region
Transmembrane domain
Intracellular domain
TM/IC
TM/IC (- or ala)
QFKNKTGPQPVTYYKRPVQEWV
B
Cell survival (A.U.)
pcDNA
TM/IC
TM/IC-KNKTG
TM/IC-QPVT
TM/IC-YK
TM/IC-PVQ
TM/IC-EWV
TM/IC(ala)KNKTG
TM/IC(ala)QPVT
TM/IC(ala)YK
TM/IC(ala)PVQ
TM/IC(ala)EWV
TM/IC(ala)All
MT5-MMP-variant
C
13kDa
12kDa
42kDa
D
C99
C83
Actin
C99 levels (A.U.)
MT5-MMP variant
E
Aβ40 fold change vs pcDNA
F
DMSO LACT D6
TM/IC
Inhibitor
G
TM/IC(ala)KNKTG
I
TM/IC(ala)EWV

Fig 3.

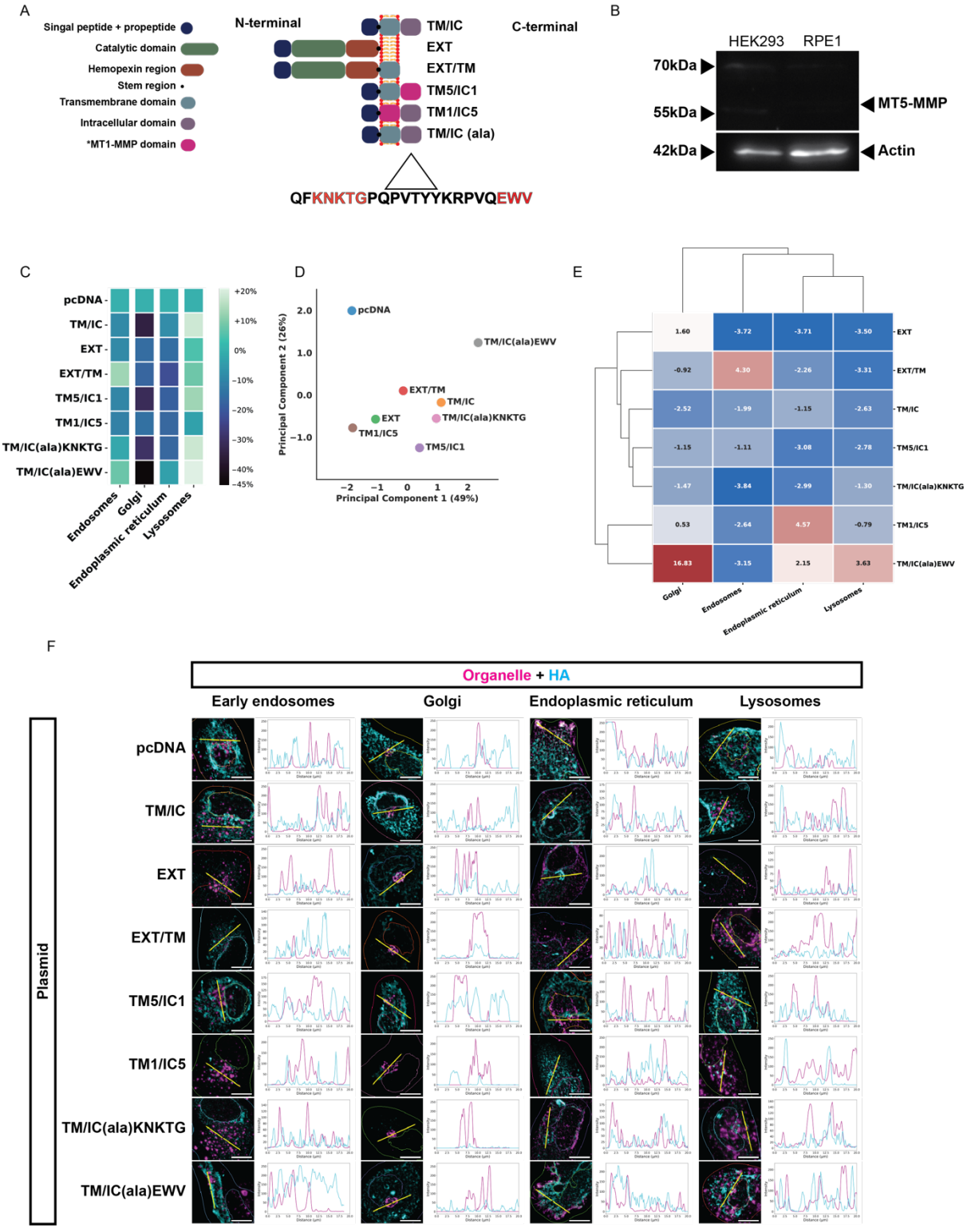
A
Singal peptide + propeptide
Catalytic domain
Hemopexin region
Stem region
Transmembrane domain
Intracellular domain
*MT1-MMP domain
N-terminal
C-terminal
TM/IC
EXT
EXT/TM
TM5/IC1
TM1/IC5
TM/IC (ala)
QFKNKTGPQPVTYYKRPVQEWV
B
HEK293
RPE1
70kDa
55kDa
42kDa
MT5-MMP
Actin
C
pcDNA
TM/IC
EXT
EXT/TM
TM5/IC1
TM1/IC5
TM/IC(ala)KNKTG
TM/IC(ala)EWV
+20%
+10%
0%
−10%
−20%
−30%
−40%
−45%
Endosomes
Golgi
Endoplasmic reticulum
Lysosomes
D
Principal Component 2 (26%)
Principal Component 1 (49%)
E
F
Organelle + HA
Early endosomes
Golgi
Endoplasmic reticulum
Lysosomes
Plasmid

Fig 4.

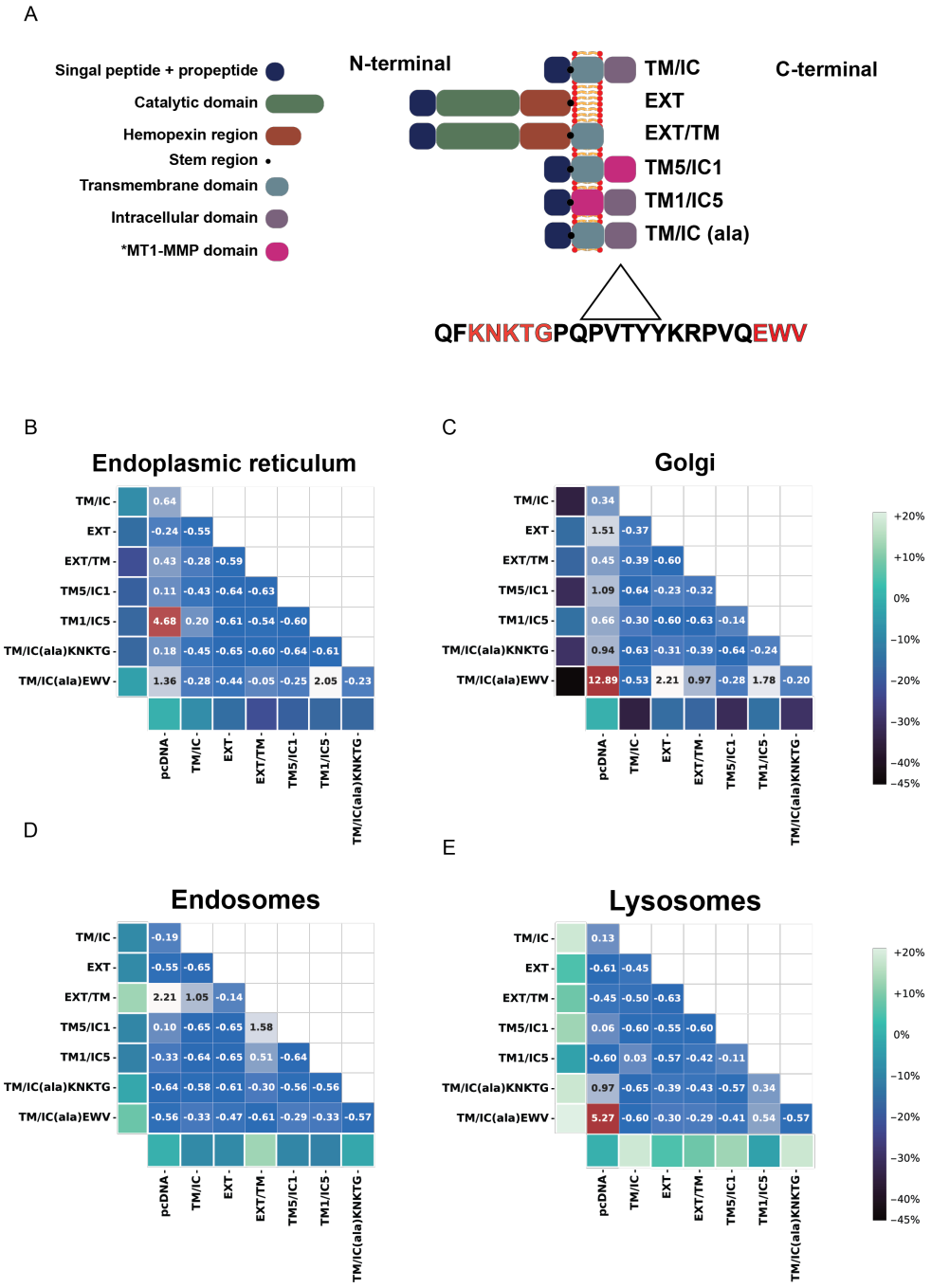
A
Singal peptide + propeptide
Catalytic domain
Hemopexin region
Stem region
Transmembrane domain
Intracellular domain
*MT1-MMP domain
N-terminal
TM/IC
EXT
EXT/TM
TM5/IC1
TM1/IC5
TM/IC (ala)
C-terminal
QFKNKTGPQPVTYYKRPVQEWV
B
Endoplasmic reticulum
C
Golgi
D
Endosomes
E
Lysosomes
TM/IC
EXT
EXT/TM
TM5/IC1
TM1/IC5
TM/IC(ala)KNKTG
TM/IC(ala)EWV
pcDNA
+20%
+10%
0%
−10%
−20%
−30%
−40%
−45%

Fig 5.

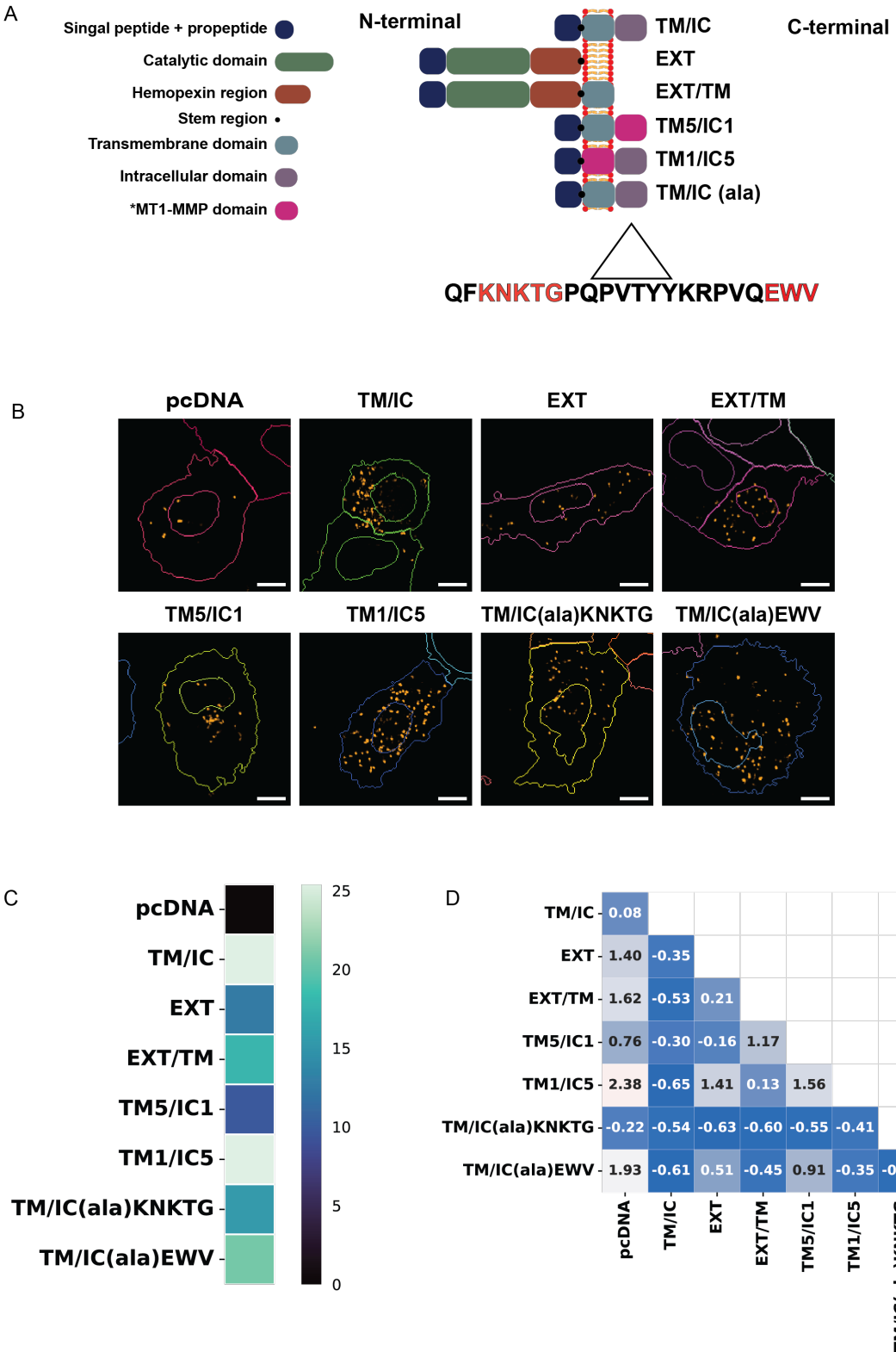
A
Singal peptide + propeptide
Catalytic domain
Hemopexin region
Stem region
Transmembrane domain
Intracellular domain
*MT1-MMP domain
N-terminal
C-terminal
TM/IC
EXT
EXT/TM
TM5/IC1
TM1/IC5
TM/IC (ala)
QFKNKTGPQPVTYYKRPVQEWV
B
pcDNA
TM/IC
EXT
EXT/TM
TM5/IC1
TM1/IC5
TM/IC(ala)KNKTG
TM/IC(ala)EWV
C
pcDNA
TM/IC
EXT
EXT/TM
TM5/IC1
TM1/IC5
TM/IC(ala)KNKTG
TM/IC(ala)EWV
25
20
15
10
5
0
D
TM/IC 0.08
EXT 1.40 -0.35
EXT/TM 1.62 -0.53 0.21
TM5/IC1 0.76 -0.30 -0.16 1.17
TM1/IC5 2.38 -0.65 1.41 0.13 1.56
TM/IC(ala)KNKTG -0.22 -0.54 -0.63 -0.60 -0.55 -0.41
TM/IC(ala)EWV 1.93 -0.61 0.51 -0.45 0.91 -0.35 -0.58
pcDNA
TM/IC
EXT
EXT/TM
TM5/IC1
TM1/IC5
TM/IC(ala)KNKTG

Figure 6.

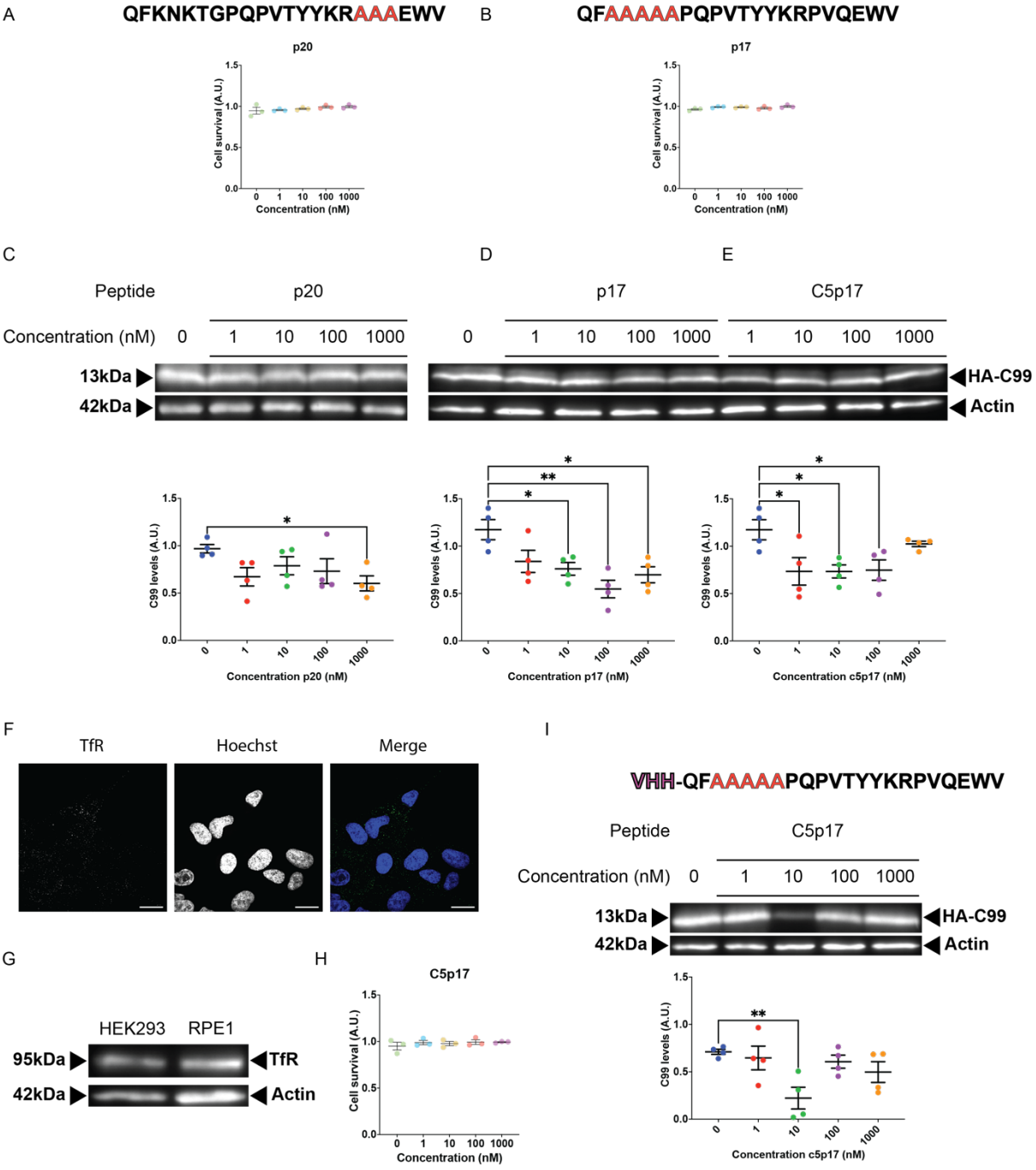
A
QFKNKTGPQPVTYYKRAAAEWV
p20
Cell survival (A.U.)
Concentration (nM)
B
QFAAAAAPQPVTYYKRPVQEWV
p17
C
Peptide
p20
Concentration (nM)
13kDa
42kDa
C99 levels (A.U.)
Concentration p20 (nM)
D
p17
C5p17
HA-C99
Actin
Concentration p17 (nM)
Concentration c5p17 (nM)
F
TfR
Hoechst
Merge
G
HEK293
RPE1
95kDa
TfR
42kDa
Actin
H
C5p17
I
VHH-QFAAAAAPQPVTYYKRPVQEWV